Identification of new phosphodiesterase 9A (PDE9A) isoforms and how their expression and subcellular compartmentalization in brain changes across the lifespan

Neema S. Patel[1], **Jennifer Klett**[1], **Katy Pilarzyk**[1], **Dong ik Lee**[2], **David Kass**[2], **Frank S. Menniti**[3], and **Michy P. Kelly**[1,*]

[1]Department of Pharmacology, Physiology & Neuroscience, University of South Carolina School of Medicine, Columbia, SC, 29209

[2]Division of Cardiology, Department of Medicine, Department of Pharmacology and Molecular Sciences, Johns Hopkins University School of Medicine, Baltimore MD 21205

[3]George and Anne Ryan Institute for Neuroscience, University of Rhode Island, Kingston, RI 02881

Abstract

$3',5'$-cyclic nucleotide phosphodiesterases (PDEs) degrade cAMP and cGMP, with PDE9A having the highest affinity for cGMP. We show PDE9A6 and three novel PDE9 isoforms (PDE9X-100, PDE9X-120, PDE9X-175) are reliably detected in brain and lung of mouse, while PDE9A2 and other isoforms are found elsewhere. PDE9A localizes to the membrane in all organs except bladder, where it is cytosolic. Brain additionally shows PDE9 in the nuclear fraction. PDE9A mRNA expression/localization dramatically changes across neurodevelopment in a manner that is strikingly consistent between mouse and human (i.e., decreased expression in hippocampus and cortex, inverted-U in cerebellum). Study of the four PDE9 isoforms in mouse brain from postnatal day 7 through 24 months similarly identifies dramatic effects of age on expression and subcellular compartmentalization that are isoform- and brain region-specific. Finally, PDE9A mRNA is elevated in the aged human hippocampus with dementia when there is a history of traumatic brain injury. Thus, brain PDE9 is localized to preferentially regulate nuclear- and membrane-proximal pools of cGMP, and its function likely changes across the lifespan.

*corresponding author: Michy P. Kelly, Ph.D., Department of Pharmacology, Physiology & Neuroscience, University of South Carolina School of Medicine, 6439 Garners Ferry Road, VA Bldg 1, 3rd Floor, D-12, Columbia, SC 29209, Phone: 803-216-3546, Fax: 803-216-3551.

Keywords

phosphodiesterase; hippocampus; cerebellum; prefrontal cortex; striatum; GAPDH; ponceau; Allen Institute for Brain Science; cGMP; aging; granule cell; molecular layer; aging; development; purkinje

1. Introduction

The phosphodiesterases (PDEs) are a superfamily of enzymes that metabolize and inactivate the intracellular second messengers cAMP and/or cGMP (Conti and Beavo, 2007, Francis et al., 2011). PDEs are grouped into 11 families based on homology of the catalytic domains. PDEs are discretely localized to specific subcellular domains (Houslay, 2010, Kokkonen and Kass, 2017). As a result, PDEs do not simply control the total cellular content of cyclic nucleotides, they generate individual pools or nanodomains of cyclic nucleotide signaling. Such subcellular compartmentalization of cyclic nucleotide signaling allows a single cell to respond systematically to diverse intra- and extracellular signals. Given the physiological significance of the PDE superfamily, and the facility with which it has been possible to discover family-specific inhibitors, the PDEs are of significant interest in the quest for novel therapeutics (Lugnier, 2006, Menniti et al., 2006). To fully understand the potential of a given PDE as a therapeutic target, however, we must first understand which pool of cyclic nucleotides it controls.

The focus of this report is PDE9A, a cGMP-specific PDE coded by a single gene that is alternatively spliced to generate more than 20 isoforms (Fisher et al., 1998, Rentero et al., 2003, Wang et al., 2003, Kotera and Omori, 2006). Of all the cGMP-specific PDEs, PDE9 has the highest affinity for cGMP (Singh and Patra, 2014). cGMP is produced by either a particulate guanylyl cyclase (pGC) or a soluble guanylyl cyclase (sGC) (Castro et al., 2006). The pGC is present at the plasma membrane and activated by natriuretic peptides, and sGC is present in the cytosol where it is activated by nitric oxide (NO) (Castro et al., 2006). Recent studies in cardiac tissue showed that PDE9A regulates pools of cGMP downstream of natriuretic peptide activated pGC, not pools of cGMP downstream of nitrous oxide (NO) activated sGC (Lee et al., 2015). These findings suggest that PDE9A is likely to be enriched in the membrane, but this has yet to be established.

Pde9a mRNA is expressed throughout the body and the brain (Lakics et al., 2010). In situ hybridization studies of the rodent brain indicate the highest level of *Pde9a* mRNA are found in Purkinje neurons of the cerebellum, with much lower levels found in cortex (particularly layer 5), the pyramidal cell layer of the hippocampus, and the striatum (Andreeva et al., 2001, van Staveren and Markerink-van Ittersum, 2005, Kelly et al., 2014). Genetic deletion or pharmacological inhibition of PDE9A are sufficient to cause a robust increase in cGMP throughout forebrain and cerebellum, indicating the enzyme regulates an active cGMP signaling cascade (Hutson et al., 2011, Kleiman et al., 2012). PDE9A inhibition also increases cGMP in CSF of both rodents and humans (Nicholas et al., 2009, Schmidt et al., 2009, Boland et al., 2017), suggesting at least partial conservation of PDE9A regulated cGMP signaling across species.

In the brain, PDE9A-regulated cGMP signaling appears to be involved in some forms of synaptic plasticity. Several groups have reported that PDE9A inhibition facilitates induction of long-term potentiation at the hippocampal CA3/CA1 synapse (Hutson et al., 2011, Kroker et al., 2012, Kroker et al., 2014). These same investigators and others have reported the ability of PDE9A inhibitors to improve cognitive function in rodents (van der Staay et al., 2008, Hutson et al., 2011, Vardigan et al., 2011, Kleiman et al., 2012, Alexander et al., 2016). Supported by these findings, PDE9A inhibitors have been advanced into clinical trials to assess their potential for improving cognitive function in patients with Alzheimer's disease and schizophrenia (Schwam et al., 2014, Wunderlich et al., 2016, Boland et al., 2017). Although Pfizer's PDE9 inhibitor PF-04447943 was generally well-tolerated, it failed to improve the cognition or behavior of Alzheimer's patients (Schwam et al., 2014). More recently, PDE9A inhibition ameliorated auditory gating deficits in the *Bachd* transgenic rat model of Huntington's disease (Nagy et al., 2015) and reduced a social withdrawal deficit in dystrophin-deficient mice, a model of an autism-like behavioral deficit associated with Duchenne muscular dystrophy (Alexander et al., 2016). In considering PDE9A as a therapeutic target for an age-related disease such as Huntington's vs. a neurodevelopmental disorder such as autism, it is interesting to note that cGMP levels dramatically increase between postnatal day (PD) 10 and adulthood in the rodent cerebellum (Steiner et al., 1972). This, along with a qualitative study of *Pde9a* mRNA expression in rat brain (Van Staveren et al., 2003), suggests that PDE9 protein expression in the cerebellum might substantially decrease during postnatal development.

It has yet to be reported which pools of cGMP are regulated by PDE9A in brain. Given that diseases such as Alzheimer's disease have been associated with subcellular compartment-specific deficits in cGMP signaling (Bonkale et al., 1995, Kelly, 2018), it is important to address this gap in knowledge. As such, this study aims to identify 1) the subcellular localization of PDE9 isoforms in the brain and 2) how PDE9 expression and subcellular localization of PDE9A may change across the lifespan. We show here that PDE9 in brain is enriched in the membrane (i.e. in proximity to pGC) and nuclear compartments relative to the cytosol and that PDE9 expression and subcellular compartmentalization dramatically change across the lifespan in a manner that is isoform and brain region specific.

2. Methods and Materials

2.1 Subjects

Pde9a KO mice were originally developed by Pfizer Inc. and maintained on a mixed C57BL/6J-C57BL/6N background. The *Pde9a KO* deletion targets the catalytic domain (Lee et al., 2015), therefore all PDE9A isoforms are targeted (Rentero et al., 2003). For these studies, *Pde9a* wild-type (WT) and KO mice were obtained from heterozygous (HT) × HT matings maintained at John Hopkins University. Subjects were 2-4 months old and equal numbers of males and females were included. For the developmental study, postnatal day 28 (P28) vs. young adult study (2-4 months old), and young adult vs. old adult study (22-24 months old), approximately equal numbers of male and female C57BL/6J mice were used (see figure legends for specific n's used in each study). The C57BL/6J mice were bred and maintained at the University of South Carolina (strain originally obtained from Jackson

Laboratories—Bar Harbor, ME). Experiments were carried out in accordance with the National Institutes of Health Guide for the Care and Use of Laboratory Animals (Pub 85-23, revised 1996) and were fully approved by the Institutional Animal Care and Use Committee of the University of South Carolina and Johns Hopkins University.

2.2 Western blotting

For all biochemical/molecular studies, *Pde9a WT* and KO mice were anesthetized by isoflurane and then killed by cervical dislocation, and C57BL/6J mice were killed by cervical dislocation without anesthesia. The difference in euthanasia methods was due to the different protocols employed by the Johns Hopkins vs. University of South Carolina research teams, respectively. Western blots were conducted as previously described (Hegde et al., 2016a, Hegde et al., 2016b, Pathak et al., 2017) by loading equal amounts of total protein for each sample (33 μg for each total homogenate sample, 22μg for each fractionated sample) onto NuPAGE Novex 4-12% Bis-Tris polyacrylamide gradient gels (Life Technologies NP0323BOX—Carlsbad, CA). Protein was transferred to nitrocellulose membranes that were probed overnight at 4°C for PDE9A using custom rabbit polyclonal antibodies ("13128-5"and "13128-6,7" at 1:8500 in 5%milk/0.1% Tween—gifts from Laurinda A. Jaffe; "18092 AP" at 1:8500 in 5%milk/0.1% Tween—generated by the Kass lab). These polyclonal antibodies were raised against amino acids 181-506 of the PDE9A2 catalytic domain (antigen described by (Huai et al., 2004)) and then affinity purified by ProSci Inc (Poway, CA). Membranes were also stained by ponceau and probed for GAPDH (1:10,000 in Superblock/0.1% Tween; Sigma G8795—St. Louis, MO) to assess protein loading. Membranes were placed in a cassette and multiple film exposures were taken to ensure data were collected within the linear range. The optical densities from Western blot and ponceau stains were quantified using Image J (NIH) (sample minus background).

2.3 Immunofluorescence (IF) and immunohistochemistry (IHC)

Brains were cryosectioned at 20 μm, and slides then underwent fixation (4% paraformaldehyde/1× phosphate-buffered saline) and antigen retrieval (10mM Citrate Buffer/0.05% Tween 20 at pH 6.0 heated to 90°C). Slides were then processed for IF and IHC as previously described (Hegde et al., 2016a) using antibodies against PDE9A (1:5000 of 13128-5) and glial fibrillary acid protein (GFAP; 1:500 of Aves GFAP—Tigard, OR) or NF-H (1:2000 of Cell Signaling RMD020— Dancers, MA). The PDE9A antibodies were diluted in 5% milk/0.02% NaN3/PBT with the rest diluted in 0.02% NaN3/PBT.

2.4 Biochemical fractionation

Brain regions from *Pde9a WT* and KO mice were fractionated in parallel as previously described (Pathak et al., 2017), as were brain regions from the various C57BL/6J age groups. PDE9X-175 was more reliably detected when the lysis buffer was prepared with a singular protease/phosphatase inhibitor tablet (e.g., Pierce #88668 or #A32959 from Thermoscientific, Rockford, IL— used for Cohort 2 in the P7-P28 study) vs. a separate protease inhibitor tablet plus a liquid phosphatase inhibitor cocktail (Pierce #8865 from Thermoscientific plus #P0044 from Sigma-Aldrich, St. Louis, MO—used for Cohort 1 in the P7-P28 study).

2.5 *In-situ* hybridization

Slides were processed by autoradiographic in situ hybridization as previously described (Kelly et al., 2014, Hegde et al., 2016a) using 35S-dATPα-labeled oligonucleotide antisense/sense probes that target a region common to all *Pde9a* isoforms (antisense: 5′-tgcggagcgtgattgggttgatgctgaagtccctgaccag-3′).

2.6 Human expression data

To assess PDE9A mRNA expression in human tissue, databases from the Allen Institute for Brain Science were accessed. To examine expression of PDE9A across brain development, we collected data and heatmaps from the © 2014 Allen Institute for Brain Science BRAINSPAN Atlas of the Developing Human Brain data at http://www.brainspan.org/rnaseq/searches?exact_match=true&search_term=PDE9A&search_type=gene&page_num=0. We focused on the hippocampus, striatum, cerebellum, and prefrontal cortical areas for consistency with the brain regions we assessed in mouse. Methods employed for this RNA sequencing study have been previously published (Miller et al., 2014) and can be found here: http://help.brain-map.org/display/devhumanbrain/Documentation. Guided by our findings in mice, we grouped subjects into the following age categories prior to analyses: prenatal, childhood (2 months-17 years old), and adulthood (18-40 years old). Given that the oldest subject in the BRAINSPAN study was 40 years old, a comparison of young adult vs. old adult was not possible. As such, we also examined expression of PDE9A in the © 2016 Allen Institute for Brain Science Aging, Dementia and TBI study, a study conducted in a cohort of adults 75-100+ years old. Data for the entire study were downloaded from http://aging.brain-map.org/download/index, and the methods for this RNA sequencing study can be found here: http://help.brain-map.org/display/aging/Documentation). Heatmaps specifically of normalized PDE9A expression were accessed at http://aging.brain-map.org/rnaseq/searches?{%22exact_match%22:true,%22search_term%22:%22PDE9A%22,%22search_type%22:%22ge ne%22,%22features%22:[],%22tumors%22:[],%22page_num%22:0}.

2.7 Data analyses

Technical variables were counterbalanced across biological variables and the data were analyzed using Sigmaplot 11.1. As previously described (Kelly et al., 2014, Hegde et al., 2016a, Hegde et al., 2016b, Pathak et al., 2017), data from each Western blot were normalized to a control group (e.g., hippocampus or P28), to remove the influence of non-specific technical confounds that exist between blots (e.g. differences in film exposures). The effect of brain region, isoform, sex and/or age were analyzed by an analysis of variance (ANOVA), repeated measure ANOVA, Student's t-test, or paired t-test where data met assumptions of normality and equal variance. Where datasets failed equal variance or normality, nonparametric tests (ANOVA on Ranks, Mann Whitney Rank Sum, Wilcoxon Rank test) were used. *Post hoc* analyses were conducted using Student-Newman-Keuls Method. As previously described (Kelly et al., 2009, Kelly et al., 2014, Pathak et al., 2015, Hegde et al., 2016a, Hegde et al., 2016b, Pathak et al., 2017), statistical outliers greater than 2 standard deviations from the mean were removed from analysis (outliers/total data points:

Figure 2B, 4/64; Figure 8F, 1/48; Figure 10E, 5/94; Figure 10F 4/94) and significance was defined as P 0.05. Data were graphed as mean +/- SEM.

3. Results

3.1 PDE9A6/13 and three novel PDE9 isoforms are identified in brain and lung

To identify which PDE9 isoforms are expressed in brain, denaturing Western blots of PDE9 WT and KO cerebellum were conducted using 3 separate antibodies raised to the PDE9A catalytic domain (Figure 1A). With all 3 antibodies, a band of ~57 kDa was present in samples from *Pde9a* WT but not *Pde9a* KO mice, putatively corresponding to the molecular weight of the previously characterized PDE9A6 and PDE9A13 isoforms (see Table 1; (Rentero et al., 2003, Wang et al., 2003). Note that the isoform named "PDE9A5" in Wang et al., corresponds to the isoform named "PDE9A6" in Rentero et al. Since the molecular weights of PDE9A6 and A13 are indistinguishable on our blots, we will collectively refer to this band as PDE9A6/13. Unexpectedly, 3 additional bands could be detected in the *Pde9a* WT mice vs *Pde9a* KO mice with all 3 antibodies—these bands migrated at ~100 kDa, ~120 kDa, and ~175 kDa (Figure 1A). These bands run at a higher molecular weight than the largest known mouse (PDE9A2, ~62 kDa, (van Staveren et al., 2002)) or human PDE9A isoform (PDE9A1, ~70kDa, (Wang et al., 2003)) (Table 1). Note that only PDE9A antibodies revealed bands that were present in PDE9A WT mice but disappeared in PDE9A KO mice (see Supplement Figure 1). Although we did successfully identify the 4 isoforms with all 3 antibodies, performance of 18092 AP was less reliable, therefore detailed analyses were conducted using 13128-5 and then 13128-6,7 once 13128-5 was depleted (see figure legends for specification of antibody used).

Given that the Westerns were run under denaturing conditions, it is highly unlikely the high molecular weight bands represent a PDE9A dimer or aggregate. That said, the band running at ~120 kDa does run close to the approximate molecular weight of a PDE9A6 or PDE9A13 dimer, and it is known that PDE9A isoforms homodimerize (Yang et al., 2016). Thus, we tested whether the presence of these novel entities could be altered by applying different heating conditions to the samples. Applying high/prolonged heat to samples normally favors unfolding, however, certain proteins have actually been shown to form dimers under such conditions (Jorgensen et al., 2003). Therefore, we compared our typical denaturing condition (90°C for 2 minutes) vs. 2 prolonged heat conditions (37°C for 30 minutes and 90°C for 30 minutes) and a no heat condition. All 3 novel high molecular weight entities remained present in samples from *Pde9a WT* mice and absent in samples from *Pde9a KO* mice across the different heating conditions; however, the bands at ~175 kDa did appear to weaken somewhat when heated for 30 minutes at 90°C (Figure 1C). The fact that the bands remain stable across heating conditions argues these bands do not represent a PDE9A dimer or aggregate.

Additional PDE9A isoforms may exist in the brain, but the limited specificity of the antibodies tested here may obscure our ability to visualize a specific signal (i.e., a signal that is present in WT but absent in KO). Indeed, the intensity of bands detected by the antibody at 62 kDa, 98 kDa, 110 kDa, and 175 kDa are significantly decreased in the PDE9A KO cerebellum and/or hippocampus relative to WT (Figure 1C). Importantly, the novel PDE9A

isoforms can also be detected in lung, but not eye, liver, heart, skeletal muscle, bladder, or kidney (Figure 1D), suggesting their expression is relatively restricted in the body. For all tissues examined, PDE9A appears to be enriched in membrane fractions. A notable exception is bladder, where PDE9A is uniquely enriched in cytosol (Figure 1D), and brain, where PDE9 isoforms are also found abundantly expressed in nuclear fractions (Figure 2B). Although we have not sequenced these proteins, the fact that they are absent in PDE9A KO tissue and are not detected with antibodies to other PDE families (Supplemental Figure 1) argues they are novel PDE9 isoforms resulting from either a novel splicing of the *Pde9a* gene or a novel *Pde9* gene that has yet to be identified (i.e. *Pde9b*). Heretofore, we refer to these novel isoforms as PDE9X-100 (migrating ~100kDa), PDE9X-120 (migrating ~120kDa), and PDE9X-175 (migrating ~175 kDa).

3.2 PDE9 is enriched in cerebellum relative to other brain regions

Previously, *Pde9a* mRNA was shown to be enriched in cerebellum relative to other brain regions, including the hippocampus (Andreeva et al., 2001, Lakics et al., 2010, Kelly et al., 2014). To see if this particular enrichment translated at the protein level, denaturing Western blots of PDE9 WT and KO cerebellum and hippocampus total homogenates were first performed. PDE9A6/13, PDE9X-100, PDE9X-120, and PDE9X-175 were detected in the hippocampus as they were in cerebellum (Figure 2A), although the hippocampus did exhibit a higher background signal vs. cerebellum due to a non-specific signal emanating from the nuclear fraction (Figure 2B). Thus, interpretation of PDE9X-175 labeling in hippocampus vs. cerebellum should be made with this confound in mind.

In both the cerebellum and hippocampus, the signal for the PDE9A6/13 band was much more intense than those for the upper isoforms (PDE9A6/13 ≫ PDE9X-120 > PDE9X-175 > PDE9X-100). Indeed, PDE9X-100 expression was so low we were often unable to reliably detect it in fractionated samples due to the lower protein concentration. Therefore, different film exposures were required to visualize each isoform within the linear range of the film. To account for this technical difference across bands, data for each isoform were normalized to the hippocampus and the relative enrichment of each band in cerebellum vs. hippocampus was compared across isoforms. Interestingly, only 2 of the 4 PDE9 isoforms were enriched in the cerebellum relative to hippocampus (Figure 2A). PDE9X-120 is expressed almost 3-fold higher in cerebellum vs. hippocampus and PDE9A6/13 is expressed 4-fold higher in cerebellum vs. hippocampus, indicating that the magnitude of the regional enrichment of PDE9 in cerebellum vs. hippocampus is isoform specific (Figure 2A).

3.3 PDE9 is enriched in membrane and nuclear subcellular fractions

To further characterize the subcellular compartmentalization of each PDE9 isoform, biochemical fractionations followed by denaturing Western blots were performed. In hippocampus and cerebellum, all three isoforms were enriched in the nuclear and membrane fractions relative to the cytosol (Figure 2B). The cerebellar nuclear:membrane ratio of each isoform was approximately 1, showing an equal distribution between these 2 compartments (Figure 2B). In contrast, the hippocampal nuclear:membrane ratio for 3 of the 4 isoforms ranged from 2 to 4, showing a significant enrichment in the nucleus relative to the membrane (Figure 2B). This shows that PDE9 is compartmentalized differently in cerebellum vs.

hippocampus of *PDE9A WT* mice. Indeed, the nuclear:membrane ratio of each isoform was significantly lower in the cerebellum vs. hippocampus (Figure 2B). Interestingly, the magnitude of the nuclear:membrane ratio of PDE9X-100 in hippocampus was higher than that of the other PDE9 isoforms within this region (Figure 2B). This suggests that the subcellular distribution of PDE9 is both region specific and isoform specific.

3.4 PDE9 is enriched in Purkinje neurons of the cerebellum

Given that PDE9 protein expression is enriched in the cerebellum, we next used immunofluorescence (IF) to investigate which cells within the cerebellum— and what compartments within those cells—express PDE9A protein. A previous study suggested PDE9A protein expression is enriched in Purkinje cells (Kleiman et al., 2012), but they lacked tissue from PDE9A KOs to confirm specificity of the signal. Indeed, our PDE9 IF signals in hippocampus did not reliably differ between *Pde9a* WT and KO brains; therefore, only cerebellum was analyzed by this method. By comparing staining in cerebellum of adult PDE9 WT vs KO mice, we confirmed that PDE9 protein is enriched in the Purkinje cell layer (clearly identifiable due to the unique morphology of these cells and NF-H staining (Demilly et al., 2011)), with additional weak expression observed in the granular and molecular layers (Figure 3A-B). A closer look at the Purkinje cell layer shows that PDE9 protein does not colocalize with the astrocyte marker GFAP (Figure 3B) but does colocalize with the neurofilament protein NF-H in Purkinje cell bodies (Figure 3B). There was no evidence of dendritic or axonal expression of PDE9A.

3.5 PDE9 expression and subcellular compartmentalization dramatically change across early postnatal development

To quantify how expression of PDE9 might change during early postnatal development in the mouse brain, brains were collected from C57BL/6J mice at various time points. For Cohort 1, brains were collected at P7, P14, P21 and P28 (P7-P28). One hemisphere was kept intact for autoradiographic *in situ* hybridization to assess *Pde9a* mRNA (Figure 4) and the other was dissected to analyze PDE9 protein expression by Western blot (Figure 5). For Cohort 2, brains were collected and dissected at P7, P14 and P28 to expand upon the biochemical data collected for specific brain regions (e.g., to measure compartmentalization where only expression data had been collected) and to assess the reproducibility of effects noted in Cohort 1. Findings were generally consistent between Cohorts 1 and 2, so combined data analyses are presented where data were collected from both cohorts. *Pde9a* mRNA expression in CA3 and CA1 of hippocampus, subiculum, and cortex dramatically decreases between P7 and P28 (Figure 4A-B). This is similar to what was qualitatively described in the rat brain (Van Staveren et al., 2003). In contrast, *Pde9a* mRNA expression in the cerebellum and olfactory tubercle demonstrates an inverted-U shape, where expression peaks at either P14 or P21 and significantly drops by P28 (Figure 4A-B). In addition to changes in total levels of mRNA expression, there also appears to be somewhat of a shift in the pattern of mRNA expression across the layers of the cerebellum between P7 and P28. At P7 and somewhat at P14, there appears to be *Pde9a* mRNA expression not only in the Purkinje and granule layer, but also the molecular layer and white matter. At P21 and P28, *Pde9a* mRNA expression is absent from the white matter and molecular layer. Given that the cerebellum exhibited a qualitative change in the laminar distribution of *Pde9a* mRNA

with age, we next conducted a qualitative analysis using IHC to visualize PDE9 protein (Figure 4D). Relative to the adult condition, at P7 and P14 there appears to be higher expression of PDE9 protein in the molecular layer and white matter but less expression in the Purkinje cell layer of cerebellum. As development progresses to P21 and P28, PDE9 labelling in the white matter disappears (Figure 4D inset), but the labelling in the Purkinje cell layer becomes much more robust.

We next analyzed PDE9 protein expression in cerebellum, hippocampus (includes CA1-CA3, DG, and part of subiculum), prefrontal cortex, and striatum by denaturing Western blot. All PDE9 isoforms dramatically decrease in expression between P7-14 and P28 in cerebellum (Figure 5A) and hippocampus (Figure 6A,C). In contrast, only PDEX-120, PDE9X-100, and PDE9A6/13 decrease during this window in prefrontal cortex (Figure 7A), and while PDE9X120 and PDE9X-100 decrease during this time frame in striatum, PDE9A6/13 expression in striatum actually increases between P7 and P14 (Figure 7B). Note that GAPDH expression was found to dramatically increase in expression between P7 and P28 (Supplemental Figure 2); therefore, ponceau stain was used to correct the P7-P28 total homogenates for any differences in protein loading. Together, these data suggest that the neurodevelopmental changes in PDE9 expression are isoform and brain region specific.

To determine whether the subcellular compartmentalization of PDE9 protein also changed during early postnatal development, we performed biochemical fractionation of the C57BL/6J cerebellum, hippocampus, prefrontal cortex, and striatum and blotted the nuclear and membrane fractions. Note, we did verify that our subcellular fractionation protocol worked in these younger tissues (Supplemental Figure 3). Across brain regions and isoforms, there are many instances of isoforms shifting their relative distribution between membrane and nuclear fractions. In cerebellum (Figure 5B) and prefrontal cortex (Figure 7B), PDE9X-120 and PDE9A6/13 show a significant change in their subcellular distribution between P7-14 to P21-28. Surprisingly, no isoform shows such a shift in either hippocampus (Figure 6B) or striatum (Figure 7D), showing that PDE9 isoforms are developmentally regulated in a brain region- and isoform-specific manner.

3.7 Between P28 and young adulthood, PDE9 expression and/or compartmentalization continue to change in prefrontal cortex and striatum

From P28 to young adulthood (i.e., 2-4 months old), expression of each PDE9 isoform appears to stabilize in hippocampus, cerebellum, and striatum; however, expression of PDE9A6/13 and PDE9X-120 continue to decrease in prefrontal cortex (Figure 8C). Further, within prefrontal cortex, PDE9X-100, PDE9X-120 and PDE9X-175 demonstrate a significant shift in their subcellular distribution, further strengthening their nuclear enrichment (Figure 8E). In striking contrast, striatum shows that PDE9X-175 actually shifts from a more nuclear-enriched subcellular distribution to a more membrane-enriched distribution. Thus, striatum again demonstrates a unique regulation of PDE9A.

3.8 Between young and old adulthood, PDE9 expression and/or compartmentalization continue to change inprefrontal cortex and striatum

Consistent with our previous assessment of young vs. aged adulthood *Pde9a* mRNA expression in rat (Kelly et al., 2014), there are no significant changes in PDE9 protein expression in hippocampus, cerebellum, prefrontal cortex nor striatum between young (2-4 months old) and late adulthood (22-24 months old), with the exception of PDE9X-175 showing a slight reduction in prefrontal cortex (Figure 9A-D). Changes in subcellular compartmentalization are also rather restricted, with changes between young and late adulthood occurring in the distribution of hippocampal PDE9X-120 and prefrontal cortex PDE9X-120 and PDE9A6/13 only (Figure 9E-H). It is important to note here that in the adult cerebellum, the relative enrichment of PDE9A6/13 in nucleus vs. membrane for C57BL/6J mice is different than what we observed for PDE9 WT mice (Figure 2A). That is, in cerebellum of adult C57BL/6J mice we consistently see an enrichment in nucleus vs. membrane (Figure 9), but in cerebellum of adult *Pde9a WT* mice we consistently see an equal distribution between nucleus and membrane (Figures 2B). This suggests that signals controlling the compartmentalization of PDE9 differ between these mouse strains or are influenced by environmental conditions that differ between the 2 animal colonies.

3.9 PDE9A expression in human closely mirrors our findings in mice

To determine if these aging effects observed in mice were conserved in human, we collected PDE9A mRNA expression data from the © 2014 Allen Institute for Brain Science—BRAINSPAN Atlas of the Developing Human Brain and the © 2016 Allen Institute for Brain Science—Aging, Dementia and TBI study. PDE9A mRNA expression patterns in the developing human brain are strikingly reminiscent of those we describe above in mouse (Figure 10A-C). Hippocampus and prefrontal cortical areas show a robust decrease in PDE9A mRNA expression between the postnatal period and childhood, with a further decrease between childhood and adulthood observed in the prefrontal cortical areas (Figure 10A-B). Although there was not a significant difference in PDE9A mRNA expression in striatum (Str) or cerebellum (Cblm) between the prenatal period and childhood, a visual inspection of the heatmaps identified a potential window during which PDE9A expression may change in these regions (i.e., between postnatal week 16 and 1 year of age). Given that PDE9A mRNA expression exhibited an inverted-U in the mouse cerebellum between P7-P28 and PDE9A6/13 expression significantly increased in mouse striatum during this period, a *post hoc* analysis was conducted breaking apart the postnatal and childhood periods into an early vs. late epoch, in order to create 3 age brackets (early postnatal, late postnatal/early childhood spanning postnatal week 16-1year of age, and later childhood beyond 1 year old). Comparison of these 3 age brackets revealed that PDE9A mRNA expression in human exhibits an inverted-U shape in cerebellum (Figure 10C), as it does in mice (Figure 4B). Although the Allen Institute has not yet compared gene expression in young vs. old adult humans, they have assessed gene expression within a cohort of adults aged 75-100+ years who have been diagnosed with a history of traumatic brain injury (TBI) and/or dementia. Within this aged population, there were significantly higher PDE9A mRNA levels in the hippocampus of individuals with a history of TBI that went on to develop dementia relative to those that did not go on to develop dementia (Figure 10D-F). Interestingly, PDE9A

mRNA was not elevated in those who were diagnosed with dementia in absence of a history of TBI.

4. Discussion

Here, we characterized the expression patterns and subcellular distribution of PDE9A6/13 as well as three novel isoforms that we provisionally name PDE9X-175, PDE9X-120 and PDE9X-100. The apparent molecular weights of these isoforms far exceed those of previously identified *Pde9a* mRNA splice variants (see Table 1). It is highly unlikely that PDE9X-120 or PDE9X-100 represent dimers or other PDE9A macromolecular complexes (Figure 1B); however, we cannot rule out the possibility that PDE9X-175 may reflect a denaturing-resistant dimer or macromolecular complex given that prolonged heat did appear to diminish expression (Figure 1B) and the buffer composition was able to affect detection of this band (see Methods). Interestingly, these isoforms appear to be relatively rare, only being detected in the brain and lung, not heart, kidney, bladder, eye, liver, muscle, or skeletal muscle. Further, the relative distribution of each isoform between subcellular compartments in brain is region, isoform, and age specific (Table 2). These novel isoforms are detected in tissue of *Pde9a* WT mice using 3 PDE9A antibodies (Figure 1A) but are absent in tissue from *Pde9a* KO mice, arguing for their authenticity as novel PDE9 isoforms. These novel PDE9A isoforms may result from either a novel and highly homologous *Pde9* gene that has yet to be identified (e.g., *Pde9b*) or an unreported alternative splicing of the *Pde9a* gene that includes novel exons. Indeed, precedence exists for the latter suggestion as a new "exon 6" was identified several years after the initial cloning of PDE9A (Bingham et al., 2006). Further, 16 novel PDE10A exons (many formerly identified as introns) have just recently been discovered (MacMullen et al., 2016, MacMullen et al., 2017), suggesting there is more to learn about the genetic architecture of PDEs. In this regard, it is interesting to note that PDE9A has always been considered a unique cGMP-PDE due to its small size and apparent lack of typical PDE regulatory domains (Francis et al., 2011). Thus, it is possible these larger PDE9 isoforms may contain regulatory domains (e.g., GAF domains) that are not present in previously described PDE9A isoforms. It will be important for future studies to clone and sequence these novel isoforms in order to fully understand their function.

Our findings of age-related changes in PDE9A expression and localization are consistent with observations in the field. First, the majority of PDE9 protein is more highly expressed in the cerebellum relative to hippocampus, which places PDE9 isoforms in a position to regulate cGMP levels that are 15 times higher in cerebellum than any other brain region (Steiner et al., 1972). Second, PDE9 is highly enriched in membrane vs. cytosolic compartments of most tissues (except bladder, Figure 1D), which is consistent with PDE9 regulating pools of cGMP that are downstream of particulate guanylyl cyclases (Lee et al., 2015) but not soluble guanylyl cyclases (heart: (Lee et al., 2015); brain: personal observations John Harms and Chris Schmidt). Finally, PDE9 expression dramatically decreases following P7-14 in the mouse cerebellum, which parallels the sharp increase in cGMP levels that are seen between P10 and adulthood in the rodent cerebellum (Steiner et al., 1972). Together these data show that PDE9 is generally positioned to regulate membrane and nuclear pools of cGMP, but the relative strength of this regulation depends on the specific isoform, brain region, and age examined

4.1 PDE9 shows isoform-specific enrichment in cerebellum vs. hippocampus

To date, attempts to use immunological techniques to study the distribution of PDE9A protein have met with limited success. This has been in part due to non-specificity of available antibodies (i.e., antibodies with high background), but may also be related to PDE9A protein expression being very low. Here, concerns regarding non-specificity were mitigated by using tissue from a *Pde9a* KO as a negative control. Indeed, the amount of residual signal that is observed in the *Pde9a* KO tissue by both Western blot and immunofluorescence/immunohistochemistry underscores the absolute necessity of such negative controls and urges caution in interpreting results where KO tissue is not available for direct comparison. Western blots clearly showed enrichment of PDE9A6/13 and PDE9X-120 protein in cerebellum vs. hippocampus. In adult tissue, IF showed a strong PDE9 signal in the Purkinje cell layer and weaker signals in the granule cell and molecular layers. Unfortunately, with currently available antibodies, it is not possible to distinguish PDE9 isoforms using IF as all target the shared catalytic domain. In Purkinje cells, PDE9A colocalized with NF-H in the cell bodies, but there was no apparent colocalization in axons. The staining observed in the granule and molecular layers also appeared to be localized to cell bodies. Our findings stand somewhat in contrast to those of Kleiman and colleagues (Kleiman et al., 2012) who found in human tissue that PDE9A protein is not only in the cell bodies of the Purkinje cell but also the proximal dendrites of these neurons. In the *PDE9A* WT mouse samples, we did not observe dendritic-like expression patterns. It remains to be determined whether this difference between our studies reflects a true species difference, a non-specific signal in the human tissue, or a more limited sensitivity of our antibody.

4.2 The relative distribution of PDE9 between subcellular compartments is brain region, isoform, and age specific

In brain, all 4 PDE9 isoforms are largely found in the membrane and nucleus, with scarce to no expression in the cytosol. In contrast, PDE9A6 is exclusively expressed in cytosol when recombinantly expressed in HEK293T cells (Wang et al., 2003) and we show here several isoforms of PDE9A are expressed in the cytosol of bladder (Figure 1D). In the cerebellum of *Pde9a* WT mice, PDE9A is equally distributed between the membrane and nucleus; however, in the hippocampus PDE9A is enriched in the nucleus relative to membrane. Interestingly, the relative enrichment of PDE9X-100 in nucleus vs. membrane in hippocampus is far greater than the relative enrichment of the other isoforms (Figure 2B). Together, these results point to isoform and tissue specificity in the subcellular targeting of PDE9.

Although PDE9 isoforms are equally distributed between the membrane and nucleus in cerebellum of *Pde9a* WT mice, they are enriched in the nucleus relative to the membrane in cerebellum of adult C57BL/6J mice. This suggests that signals controlling the trafficking of PDE9 are affected either by genetic differences between these mouse strains, the different euthanasia methods employed (isoflurane vs. cervical dislocation, respectively), and/or environmental differences that exist between animal facilities (Johns Hopkins vs. University of South Carolina, respectively). Further, this suggests these signals control PDE9 isoform trafficking in a brain region-specific manner since PDE9 isoforms were enriched in nucleus vs membrane in the hippocampus of both *Pde9a* WT and C57BL/6J mice. Precedence exists

for brain region-specific genetic and environmental control of PDE compartmentalization. PDE11A4 compartmentalization in ventral hippocampus, but not dorsal hippocampus, differs between C57BL/6J mice and BALB/cJ mice (Pathak et al., 2017) as well as between group-housed and single-housed mice (Hegde et al., 2016b). In the case of PDE11A4, a difference in homodimerization explained the difference in compartmentalization that was found between C57BL/6J and BALB/cJ mice (Pathak et al., 2017).

Although C57BL/6J mice generally show enrichment of all PDE9 isoforms in the nucleus vs. membrane during adulthood, this is not true in early development. In cerebellum and prefrontal cortex, but not hippocampus nor striatum of C57BL/6J mice, PDE9A6/13 and PDE9X-120 start out equally enriched or more enriched in the membrane vs. nucleus at P7 and end up enriched in the nucleus vs. membrane by P28 (Figure 5B, 6B, 7C-D; Table 2). This shifting toward the nuclear compartment continues for PDE9X-175, PDEX-120 and PDE9X-100 in prefrontal cortex between P28 and young adulthood and for PDE9X-120 and PDE9A6/13 in prefrontal cortex between young adulthood and late adulthood (Figures 8-9; Table 2). In contrast, however, PDE9X-175 in striatum becomes less enriched in the nucleus vs. membrane between P28 and young adulthood, as does PDE9X-120 in hippocampus and PDE9X-100 in cerebellum between young and late adulthood (Figures 8-9; Table 2). Taken together, these results suggest that tissue/brain region, isoform, and age should be considered when evaluating PDE9A as a therapeutic target for a specific disease.

4.3 The expression of PDE9 is dynamically regulated during postnatal development

In addition to changes in subcellular compartmentalization, postnatal development is also accompanied by changes in PDE9 expression. We show here that the expression of *Pde9a* mRNA dramatically drops in hippocampus and cortex during the transition from the prenatal to postnatal period in both mice (note, P7 is equivalent to 3rd trimester in human; Figure 4B) and human (Figure 10A-B). Protein expression of most PDE9 isoforms similarly decreased not only in hippocampus and cortex, but also striatum and cerebellum, the latter possibly explaining the developmental increase in cGMP levels that occurs during this time in the cerebellum (Steiner et al., 1972). One notable exception to this general age-related decline in expression was a sharp increase in PDE9A6/13 expression between P7 and P14 in striatum. Among PDEs, a neurodevelopmental decrease in expression appears to be relatively unique to PDE9. *Pde11a4* mRNA and protein expression in the hippocampus dramatically increases between P7 and P28, and *Pde2a* and *Pde10a* mRNA also slightly increase between P7 and P28 (Hegde et al., 2016a). *Pde5a*, a closely related cGMP-hydrolyzing PDE that is similarly enriched in the cerebellum, does not show mRNA expression until P10 but then remains stable into adulthood (Van Staveren et al., 2003). This suggests that PDE9 is dynamically regulated during early brain development in a unique manner.

The distribution of PDE9 across the layers of the cerebellum also changes during postnatal development. PDE9 mRNA and protein appear to be expressed very strongly in the molecular layer and white matter of the cerebellum at P7, but this expression minimizes or disappears to adulthood levels by P21 (Figure 4). In this context it is interesting to note that the layers of the cerebellum are not fully mature until P20 in mice (Sillitoe and Joyner, 2007). During this period of postnatal development, the granule cell precursors are

proliferating and migrating radially into the deeper layer of cerebellar cortex to form the adult internal granule layer (Sillitoe and Joyner, 2007). Further, climbing fibers inputs to Purkinje cells are being reorganized so that by P21, Purkinje cells are innervated by only a single climbing fiber (Hashimoto et al., 2009). Thus, changes in PDE9 expression and compartmentalization may reflect and/or contribute to the establishment of proper cerebellar circuitry during early development.

4.4 Considering PDE9A as a therapeutic target

In rodents, including a mouse model of Alzheimer's disease, PDE9 inhibitors have had a positive impact on hippocampal-dependent memory and learning performances (van der Staay et al., 2008, Liddie et al., 2012, Kroker et al., 2014). These studies might suggest PDE9 inhibitors hold promise as a therapeutic approach for Alzheimer's disease. That said, reports suggest that dysfunction of sGCs, not pGCs, are found in brains of Alzheimer's patients and *in vitro* models of Alzheimer's disease pathology (Bonkale et al., 1995, Baltrons et al., 2002, Baltrons et al., 2004). Our results showing PDE9A expression is all but absent from the cytosol, suggest that PDE9 inhibitors would not be in a position to address deficits in sGC signaling (Kelly, 2018). Further, we show here that PDE9A mRNA is only increased with dementia when there is a history of TBI, not with either dementia or TBI alone (Figure 10). Indeed, Pfizer's double-blind placebo-controlled trial using a selective PDE9 inhibitor failed to elicit improvement in either cognition or dementia-related behavioral disturbances of Alzheimer's patients (Schwam et al., 2014).

If expression levels can be taken as any indication of overall enzyme function, our results here suggest a PDE9 inhibitor would more readily modulate cerebellar function compared to hippocampal function, and would more readily modulate brain function early in development as opposed to later in life. Taken together, this would suggest that PDE9 may not be the best therapeutic target for an age-related disorder of the hippocampus. Instead, it may be more relevant as a therapeutic target for a neurodevelopmental disorder such as autism. Indeed, PDE9 inhibitors have been identified as a potential therapeutic approach for DMD-associated autism (Alexander et al., 2016).

In conclusion, PDE9 is positioned to regulate membrane and nuclear pools of cGMP, but its relative distribution across subcellular compartments changes with age, isoform, mouse strain, and brain region examined. It will be of interest for future studies to clone the novel isoforms reported herein and to determine if the catalytic activity of PDE9 might also show differences across brain regions, isoforms, and age. Taken together, our results provide key insight into PDE9 function in the central nervous system.

Supplementary Material

Refer to Web version on PubMed Central for supplementary material.

Acknowledgments

References

Alexander MS, Gasperini MJ, Tsai PT, Gibbs DE, Spinazzola JM, Marshall JL, Feyder MJ, Pletcher MT, Chekler EL, Morris CA, Sahin M, Harms JF, Schmidt CJ, Kleiman RJ, Kunkel LM. Reversal of neurobehavioral social deficits in dystrophic mice using inhibitors of phosphodiesterases pde5a and pde9a. Transl Psychiatry. 2016; 6:e901. [PubMed: 27676442]

Andreeva SG, Dikkes P, Epstein PM, Rosenberg PA. Expression of cgmp-specific phosphodiesterase 9a mrna in the rat brain. J Neurosci. 2001; 21:9068–9076. [PubMed: 11698617]

Baltrons MA, Pedraza CE, Heneka MT, Garcia A. Beta-amyloid peptides decrease soluble guanylyl cyclase expression in astroglial cells. Neurobiol Dis. 2002; 10:139–149. [PubMed: 12127152]

Baltrons MA, Pifarre P, Ferrer I, Carot JM, Garcia A. Reduced expression of no-sensitive guanylyl cyclase in reactive astrocytes of alzheimer disease, creutzfeldt-jakob disease, and multiple sclerosis brains. Neurobiol Dis. 2004; 17:462–472. [PubMed: 15571982]

Bingham J, Sudarsanam S, Srinivasan S. Profiling human phosphodiesterase genes and splice isoforms. Biochem Biophys Res Commun. 2006; 350:25–32. [PubMed: 16987497]

Boland K, Moschetti V, Dansirikul C, Pichereau S, Gheyle L, Runge F, Zimdahl-Gelling H, Sand M. A phase i, randomized, proof-of-clinical-mechanism study assessing the pharmacokinetics and pharmacodynamics of the oral pde9a inhibitor bi 409306 in healthy male volunteers. Human Psychopharmacology: Clinical and Experimental. 2017; 32:e2569–n/a.

Bonkale WL, Winblad B, Ravid R, Cowburn RF. Reduced nitric oxide responsive soluble guanylyl cyclase activity in the superior temporal cortex of patients with alzheimer's disease. Neurosci Lett. 1995; 187:5–8. [PubMed: 7617301]

Castro LR, Verde I, Cooper DM, Fischmeister R. Cyclic guanosine monophosphate compartmentation in rat cardiac myocytes. Circulation. 2006; 113:2221–2228. [PubMed: 16651469]

Conti M, Beavo J. Biochemistry and physiology of cyclic nucleotide phosphodiesterases: Essential components in cyclic nucleotide signaling. Annual Review of Biochemistry. 2007; 76:481–511.

Demilly A, Reeber SL, Gebre SA, Sillitoe RV. Neurofilament heavy chain expression reveals a unique parasagittal stripe topography in the mouse cerebellum. Cerebellum. 2011; 10:409–421. [PubMed: 20127431]

Fisher DA, Smith JF, Pillar JS, St Denis SH, Cheng JB. Isolation and characterization of pde9a, a novel human cgmp-specific phosphodiesterase. Journal of Biological Chemistry. 1998; 273:15559–15564. [PubMed: 9624146]

Francis SH, Blount MA, Corbin JD. Mammalian cyclic nucleotide phosphodiesterases: Molecular mechanisms and physiological functions. Physiol Rev. 2011; 91:651–690. [PubMed: 21527734]

Hashimoto K, Yoshida T, Sakimura K, Mishina M, Watanabe M, Kano M. Influence of parallel fiber-purkinje cell synapse formation on postnatal development of climbing fiber-purkinje cell synapses in the cerebellum. Neuroscience. 2009; 162:601–611. [PubMed: 19166909]

Hegde S, Capell WR, Ibrahim BA, Klett J, Patel NS, Sougiannis AT, Kelly MP. Phosphodiesterase 11a (pde11a), enriched in ventral hippocampus neurons, is required for consolidation of social but not nonsocial memories in mice. Neuropsychopharmacology. 2016a; 41:2920–2931. [PubMed: 27339393]

Hegde S, Ji H, Oliver D, Patel NS, Poupore N, Shtutman M, Kelly MP. Pde11a regulates social behaviors and is a key mechanism by which social experience sculpts the brain. Neuroscience. 2016b; 335:151–169. [PubMed: 27544407]

Houslay MD. Underpinning compartmentalised camp signalling through targeted camp breakdown. Trends Biochem Sci. 2010; 35:91–100. [PubMed: 19864144]

Huai Q, Wang H, Zhang W, Colman RW, Robinson H, Ke H. Crystal structure of phosphodiesterase 9 shows orientation variation of inhibitor 3-isobutyl-1-methylxanthine binding. Proc Natl Acad Sci U S A. 2004; 101:9624–9629. [PubMed: 15210993]

Hutson PH, Finger EN, Magliaro BC, Smith SM, Converso A, Sanderson PE, Mullins D, Hyde LA, Eschle BK, Turnbull Z, Sloan H, Guzzi M, Zhang X, Wang A, Rindgen D, Mazzola R, Vivian JA, Eddins D, Uslaner JM, Bednar R, Gambone C, Le-Mair W, Marino MJ, Sachs N, Xu G, Parmentier-Batteur S. The selective phosphodiesterase 9 (pde9) inhibitor pf-04447943 (6-[(3s, 4s)-4-methyl-1-(pyrimidin-2-ylmethyl)pyrrolidin-3-yl]-1-(tetrahydro-2h-py ran-4-yl)-1,5-dihydro-4h-pyrazolo[3,4-d]pyrimidin-4-one) enhances synaptic plasticity and cognitive function in rodents. Neuropharmacology. 2011; 61:665–676. [PubMed: 21619887]

Jorgensen CS, Ryder LR, Steino A, Hojrup P, Hansen J, Beyer NH, Heegaard NH, Houen G. Dimerization and oligomerization of the chaperone calreticulin. Eur J Biochem. 2003; 270:4140–4148. [PubMed: 14519126]

Kelly MP, Logue SF, Dwyer JM, Beyer CE, Majchrowski H, Cai Z, Liu Z, Adedoyin A, Rosenzweig-Lipson S, Comery TA. The supra-additive hyperactivity caused by an amphetamine-chlordiazepoxide mixture exhibits an inverted-u dose response: Negative implications for the use of a model in screening for mood stabilizers. Pharmacol Biochem Behav. 2009; 92:649–654. [PubMed: 19303035]

Kelly MP, Adamowicz W, Bove S, Hartman AJ, Mariga A, Pathak G, Reinhart V, Romegialli A, Kleiman RJ. Select 3′,5′-cyclic nucleotide phosphodiesterases exhibit altered expression in the aged rodent brain. Cell Signal. 2014; 26:383–397. [PubMed: 24184653]

Kelly MP. Cyclic nucleotide signaling changes associated with normal aging and age-related diseases of the brain. Cell Signal. 2018; 42:281–291. [PubMed: 29175000]

Kleiman RJ, Chapin DS, Christoffersen C, Freeman J, Fonseca KR, Geoghegan KF, Grimwood S, Guanowsky V, Hajos M, Harms JF, Helal CJ, Hoffmann WE, Kocan GP, Majchrzak MJ, McGinnis D, McLean S, Menniti FS, Nelson F, Roof R, Schmidt AW, Seymour PA, Stephenson DT, Tingley FD, Vanase-Frawley M, Verhoest PR, Schmidt CJ. Phosphodiesterase 9a regulates central cgmp and modulates responses to cholinergic and monoaminergic perturbation in vivo. J Pharmacol Exp Ther. 2012; 341:396–409. [PubMed: 22328573]

Kokkonen K, Kass DA. Nanodomain regulation of cardiac cyclic nucleotide signaling by phosphodiesterases. Annu Rev Pharmacol Toxicol. 2017; 57:455–479. [PubMed: 27732797]

Kotera, J., Omori, K. Cyclic nucleotide phosphodiesterases in health and disease. CRC Press; 2006. Pde9.

Kroker KS, Rast G, Giovannini R, Marti A, Dorner-Ciossek C, Rosenbrock H. Inhibition of acetylcholinesterase and phosphodiesterase-9a has differential effects on hippocampal early and late ltp. Neuropharmacology. 2012; 62:1964–1974. [PubMed: 22245562]

Kroker KS, Mathis C, Marti A, Cassel JC, Rosenbrock H, Dorner-Ciossek C. Pde9α inhibition rescues amyloid beta-induced deficits in synaptic plasticity and cognition. Neurobiol Aging. 2014; 35:2072–2078. [PubMed: 24746365]

Lakics V, Karran EH, Boess FG. Quantitative comparison of phosphodiesterase mrna distribution in human brain and peripheral tissues. Neuropharmacology. 2010; 59:367–374. [PubMed: 20493887]

Lee DI, Zhu G, Sasaki T, Cho GS, Hamdani N, Holewinski R, Jo SH, Danner T, Zhang M, Rainer PP, Bedja D, Kirk JA, Ranek MJ, Dostmann WR, Kwon C, Margulies KB, Van Eyk JE, Paulus WJ, Takimoto E, Kass DA. Phosphodiesterase 9a controls nitric-oxide-independent cgmp and hypertrophic heart disease. Nature. 2015; 519:472–476. [PubMed: 25799991]

Liddie S, Anderson KL, Paz A, Itzhak Y. The effect of phosphodiesterase inhibitors on the extinction of cocaine-induced conditioned place preference in mice. J Psychopharmacol. 2012; 26:1375–1382. [PubMed: 22596207]

Lugnier C. Cyclic nucleotide phosphodiesterase (pde) superfamily: A new target for the development of specific therapeutic agents. Pharmacology & Therapeutics. 2006; 109:366–398. [PubMed: 16102838]

MacMullen CM, Vick K, Pacifico R, Fallahi-Sichani M, Davis RL. Novel, primate-specific pde10a isoform highlights gene expression complexity in human striatum with implications on the molecular pathology of bipolar disorder. Transl Psychiatry. 2016; 6:e742. [PubMed: 26905414]

MacMullen CM, Fallahi M, Davis RL. Novel pde10a transcript diversity in the human striatum: Insights into gene complexity, conservation and regulation. Gene. 2017; 606:17–24. [PubMed: 28042091]

Menniti FS, Faraci WS, Schmidt CJ. Phosphodiesterases in the cns: Targets for drug development. Nature Reviews Drug Discovery. 2006; 5:660–670. [PubMed: 16883304]

Miller JA, Ding SL, Sunkin SM, Smith KA, Ng L, Szafer A, Ebbert A, Riley ZL, Royall JJ, Aiona K, Arnold JM, Bennet C, Bertagnolli D, Brouner K, Butler S, Caldejon S, Carey A, Cuhaciyan C, Dalley RA, Dee N, Dolbeare TA, Facer BA, Feng D, Fliss TP, Gee G, Goldy J, Gourley L, Gregor BW, Gu G, Howard RE, Jochim JM, Kuan CL, Lau C, Lee CK, Lee F, Lemon TA, Lesnar P, McMurray B, Mastan N, Mosqueda N, Naluai-Cecchini T, Ngo NK, Nyhus J, Oldre A, Olson E, Parente J, Parker PD, Parry SE, Stevens A, Pletikos M, Reding M, Roll K, Sandman D, Sarreal M, Shapouri S, Shapovalova NV, Gerstein MB, Geschwind DH, Glass IA, Hawrylycz MJ, Hevner RF, Huang H, Jones AR, Knowles JA, Levitt P, Phillips JW, Sestan N, Wohnoutka P, Dang C, Bernard A, Hohmann JG, Lein ES. Transcriptional landscape of the prenatal human brain. Nature. 2014; 508:199–206. [PubMed: 24695229]

Nagy D, Tingley FD 3rd, Stoiljkovic M, Hajos M. Application of neurophysiological biomarkers for huntington's disease: Evaluating a phosphodiesterase 9a inhibitor. Exp Neurol. 2015; 263:122–131. [PubMed: 25315303]

Nicholas T, Evans R, Styren S, Qiu R, Wang EQ, Nelson F, Le V, Grimwood S, Christoffersen C, Banerjee S, Corrigan B, Kocan G, Geoghegan K, Carrieri C, Raha N, Verhoest P, Soares H. Pf-04447943, a novel pde9a inhibitor, increases cgmp levels in cerebrospinal fluid: Translation from non-clinical species to healthy human volunteers. Alzheimer's & Dementia. 2009; 5:P330–P331.

Pathak G, Ibrahim BA, McCarthy SA, Baker K, Kelly MP. Amphetamine sensitization in mice is sufficient to produce both manic- and depressive-related behaviors as well as changes in the functional connectivity of corticolimbic structures. Neuropharmacology. 2015; 95:434–447. [PubMed: 25959066]

Pathak G, Agostino MJ, Bishara K, Capell WR, Fisher JL, Hegde S, Ibrahim BA, Pilarzyk K, Sabin C, Tuczkewycz T, Wilson S, Kelly MP. Pde11a negatively regulates lithium responsivity. Mol Psychiatry. 2017; 22:1714–1724. [PubMed: 27646265]

Rentero C, Monfort A, Puigdomenech P. Identification and distribution of different mrna variants produced by differential splicing in the human phosphodiesterase 9a gene. Biochem Biophys Res Commun. 2003; 301:686–692. [PubMed: 12565835]

Schmidt CJ, Harms JF, Tingley FD, Schmidt K, Adamowicz WO, Romegialli A, Kleiman RJ, Barry CJ, Coskran TM, O'Neill SM, Stephenson DT, Menniti FS. Pde9α-mediated regulation of cgmp: Developing a biomarker for a novel therapy for alzheimer's disease. Alzheimer's & Dementia. 2009; 5:P331.

Schwam EM, Nicholas T, Chew R, Billing CB, Davidson W, Ambrose D, Altstiel LD. A multicenter, double-blind, placebo-controlled trial of the pde9a inhibitor, pf-04447943, in alzheimer's disease. Curr Alzheimer Res. 2014; 11:413–421. [PubMed: 24801218]

Sillitoe RV, Joyner AL. Morphology, molecular codes, and circuitry produce the three-dimensional complexity of the cerebellum. Annu Rev Cell Dev Biol. 2007; 23:549–577. [PubMed: 17506688]

Singh N, Patra S. Phosphodiesterase 9: Insights from protein structure and role in therapeutics. Life Sci. 2014; 106:1–11. [PubMed: 24746902]

Steiner AL, Ferrendelli JA, Kipnis DM. Radioimmunoassay for cyclic nucleotides. 3. Effect of ischemia, changes during development and regional distribution of adenosine $3',5'$-monophosphate and guanosine $3',5'$-monophosphate in mouse brain. J Biol Chem. 1972; 247:1121–1124. [PubMed: 4334493]

van der Staay FJ, Rutten K, Barfacker L, Devry J, Erb C, Heckroth H, Karthaus D, Tersteegen A, van Kampen M, Blokland A, Prickaerts J, Reymann KG, Schroder UH, Hendrix M. The novel selective pde9 inhibitor bay 73-6691improves learning and memory in rodents. Neuropharmacology. 2008; 55:908–918. [PubMed: 18674549]

van Staveren WC, Glick J, Markerink-van Ittersum M, Shimizu M, Beavo JA, Steinbusch HW, de Vente J. Cloning and localization of the cgmp-specific phosphodiesterase type 9 in the rat brain. J Neurocytol. 2002; 31:729–741. [PubMed: 14501210]

Van Staveren WC, Steinbusch HW, Markerink-Van Ittersum M, Repaske DR, Goy MF, Kotera J, Omori K, Beavo JA, De Vente J. Mrna expression patterns of the cgmp-hydrolyzing

Author Manuscript
Author Manuscript
Author Manuscript
Author Manuscript

phosphodiesterases types types 2, 5, and 9 during development of the rat brain. J Comp Neurol. 2003; 467:566–580. [PubMed: 14624489]

van Staveren WC, Markerink-van Ittersum M. Localization of cyclic guanosine 3′,5′-monophosphate-hydrolyzing phosphodiesterase type 9 in rat brain by nonradioactive in situ hydridization. Methods Mol Biol. 2005; 307:75–84. [PubMed: 15988056]

Vardigan JD, Converso A, Hutson PH, Uslaner JM. The selective phosphodiesterase 9 (pde9) inhibitor pf-04447943 attenuates a scopolamine-induced deficit in a novel rodent attention task. J Neurogenet. 2011; 25:120–126. [PubMed: 22070409]

Wang P, Wu P, Egan RW, Billah MM. Identification and characterization of a new human type 9 cgmp-specific phosphodiesterase splice variant (pde9a5). Differential tissue distribution and subcellular localization of pde9a variants. Gene. 2003; 314:15–27. [PubMed: 14527714]

Wunderlich G, Thamer C, Roehrle M, Garcia M, Frölich L, Dubois B. Study design and characteristics of two phase ii proof-of-concept clinical trials of the pde9 inhibitor bi 409306 in early alzheimer's disease. Alzheimer's & Dementia. 2016; 12:P820–P821.

Yang X, Coulombe-Huntington J, Kang S, Sheynkman GM, Hao T, Richardson A, Sun S, Yang F, Shen YA, Murray RR, Spirohn K, Begg BE, Duran-Frigola M, MacWilliams A, Pevzner SJ, Zhong Q, Trigg SA, Tam S, Ghamsari L, Sahni N, Yi S, Rodriguez MD, Balcha D, Tan G, Costanzo M, Andrews B, Boone C, Zhou XJ, Salehi-Ashtiani K, Charloteaux B, Chen AA, Calderwood MA, Aloy P, Roth FP, Hill DE, Iakoucheva LM, Xia Y, Vidal M. Widespread expansion of protein interaction capabilities by alternative splicing. Cell. 2016; 164:805–817. [PubMed: 26871637]

Highlights

- PDE9A6/13 and 3 new PDE9 isoforms (PDE9X-100, PDE9X-120, PDE9X-175) were identified inbrain and lung

- Each PDE9 isoform shows a differential enrichment in cerebellum vs. hippocampus

- All 4 isoforms are enriched in nuclear and membrane fractions vs. the cytosol

- Subcellular distribution dramatically changes across life in a region- and isoform-specific manner

- PDE9A expression dramatically changes across life in a region- and isoform-specific manner

- Age-related changes in PDE9A mRNA expression found in mouse are mirrored in humans

- PDE9A mRNA increases in human hippocampus with TBI and dementia
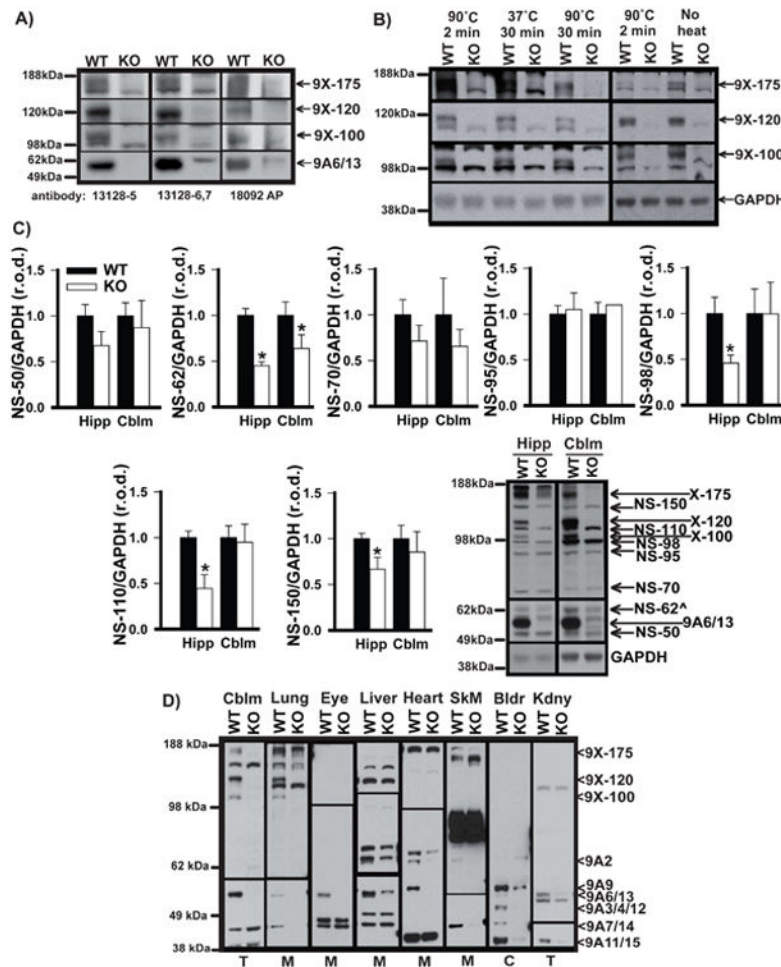
Figure 1.
Four PDE9 isoforms are expressed in the brain. A) Denaturing Western Blots of *Pde9a* wild-type (WT) and knockout (KO) cerebellum (Cblm) using 3 different custom PDE9A antibodies show the previously characterized PDE9A6/13 and three new isoforms that we name PDE9X-175, PDE9X-120 and PDE9X-100 based on their molecular weight. Note, no other previously cloned PDE9A isoforms (e.g., PDE9A2) were reliably detected in brain (that is, signal in WT and no signal in KO). B) In addition to running under denaturing conditions, we further tested if PDE9X-175, PDE9X-120 or PDE9X-100 represent a PDE9A dimer/aggregate by treating samples with prolonged heat (37°C for 30 min and 90°C for 30 min) or no heat, and compared these results to our standard denaturing condition (90°C for 2 min) using the 13128-5 antibody. The expression of PDE9X-120 and PDE9X-100 are consistent across the temperature variations, indicating these isoforms are not dimers or aggregates. Expression of PDE9X-175 did, however, appear to decrease with prolonged high heat. C) Expression of the four PDE9A isoforms was also detected in hippocampus (Hipp). To confirm that the PDE9A KO mouse does not express a truncated version of PDE9A, we overexposed the films and quantified the expression of all non-specific bands (NS) produced by the 13128-5 antibody in hippocampus (WT, n=6; KO, n=5) and cerebellum (WT and KO, n=4). There are no NS bands demonstrating increased expression in the PDE9A KO;

however, NS-62 (hipp: t(9)=6.08, P<0.001; cblm: t(3)=7.83, P=0.004), NS-98 (t(9)=2.53, P=0.032), NS-110 (t(9)=3.52, P=0.007), and NS-150 (t(9)=2.48, P=0.035) show significantly less expression in the cerebellum and/or hippocampus of the PDE9A KO vs WT mice. D) To determine if the novel PDE9A isoforms were unique to brain, we compared expression of PDE9A in cerebellum with that found in several peripheral organs using antibody 13128-6,7. Generally speaking, it was not possible to detect specific PDE9A signal in total homogenates (T, with the exception of kidney and brain); however, biochemical isolation of membrane (M) and cytosolic (C) fractions did allow for detection of specific signals in the WT vs. KO samples. Although we detected several previously cloned isoforms of PDE9A across lung, eye, liver, heart, skeletal muscle (SkM), bladder (Bldr), and kidney (Kdny), only lung showed expression of PDE9X-175, PDE9X-120, and PDE9X-100. Expression was confirmed in at least 2 WT-KO pairs, with the exception of SkM, which was only tested from 1 WT-KO pair. Note: different film exposures were required for different isoforms/tissues; therefore, black lines are used to indicate where different exposures were pasted in. Even overnight exposures of the upper bots failed to reveal expression of the novel isoforms in tissues other than brain and lung. Assignment of isoform names is based on their apparent molecular weight (see Table 1 for more information) and are consistent with a report of exon-exon junctions (Bingham et al., 2006). Panel C, n=6/geno for hipp and 4/geno for cblm. *vs. WT, P<0.04-0.001. r.o.d.—relative optical density. Brightness and contrast adjusted for graphical clarity of blot images.
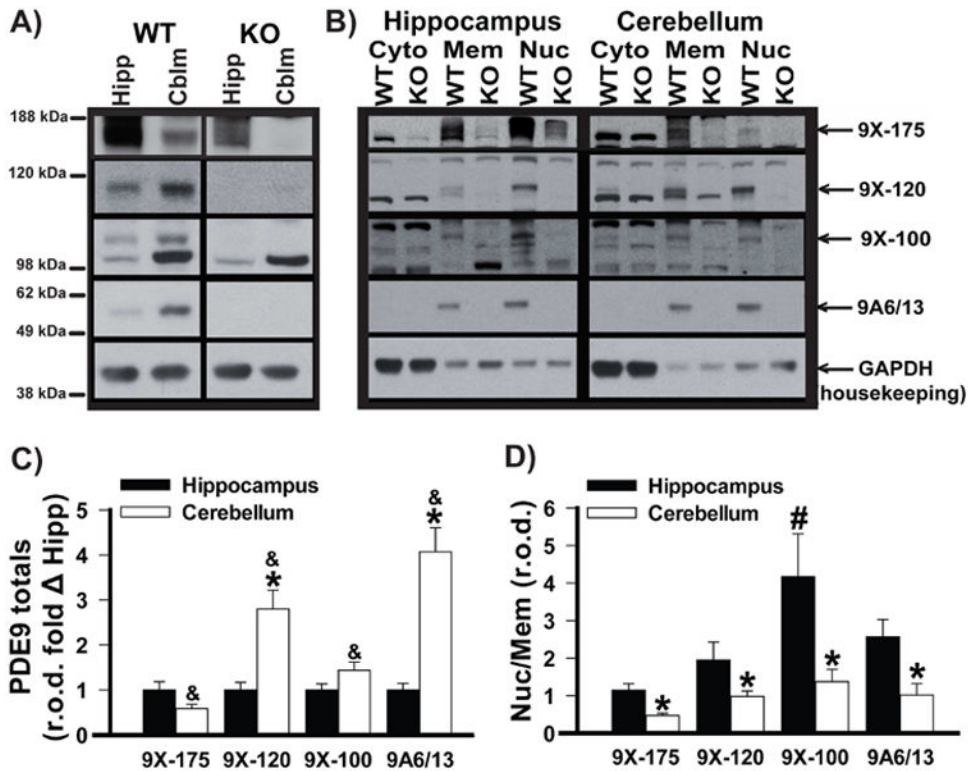
Figure 2.

The relative enrichment of PDE9A in cerebellum versus hippocampus and the relative distribution of PDE9A across subcellular fractions is brain region and isoform specific. Hippocampi (Hipp) and cerebellum (Cblm) of PDE9A wild-type (WT) and knockout (KO) mice were biochemically fractionated. Expression of PDE9A isoforms was then assessed by Western blot of A) total homogenates and B) subcellular fractions (each probed with antibody 13128-5). Note a residual non-specific signal for PDE9X-175 can be seen in hippocampus of the KO at the exposure required to visualize PDEX-175 in cerebellum. This non-specific signal is enriched in the nuclear fraction. C) PDE9X-120 (rank test: T(14)=96, P=0.002) and PDE9A6/13 (on ranks: T(14)=100, P<0.001) demonstrate a significant enrichment in the cerebellum relative to the hippocampus, consistent with previously published descriptions of *Pde9a* mRNA. PDE9X-100 shows a similar trend (on ranks: t(14)=1.89, P=0.079); whereas, PDE9X-175 shows a strong trend toward less expression in cerebellum vs. hippocampus (t(14)=2.02, P=0.063). Further, the extent to which PDE9A is enriched in cerebellum vs. hippocampus is significantly different among the isoforms (F(3,21)=38.85, P<0.001). D) Each PDE9A isoform is found in both membrane and nuclear fractions; however, the extent to which each isoform is enriched in the nucleus vs. the membrane is significantly greater in hippocampus vs. cerebellum (9X-175: t(6)=3.29, P=0.017; 9×-120: t(6)=2.82, P=0.03; 9×-100: t(5)=2.84, P=0.036; 9A6/13: t(7)=3.51, P=0.01). Further PDE9X-100 shows a significantly higher hippocampal nuclear:membrane ratio relative to the other isoforms within hippocampus (F(3,19)=4.58, P=0.014). WT— *Pde9a* wild-type; KO – *Pde9a* knockout. n=8/genotype/region. *Post hoc* *vs. Hippocampus, P<0.04-0.001; &vs. all other isoforms within cerebellum, P<0.025-0.001; #vs. PDE9X-175, P=0.009. Brightness and contrast adjusted for graphical clarity of blot images.
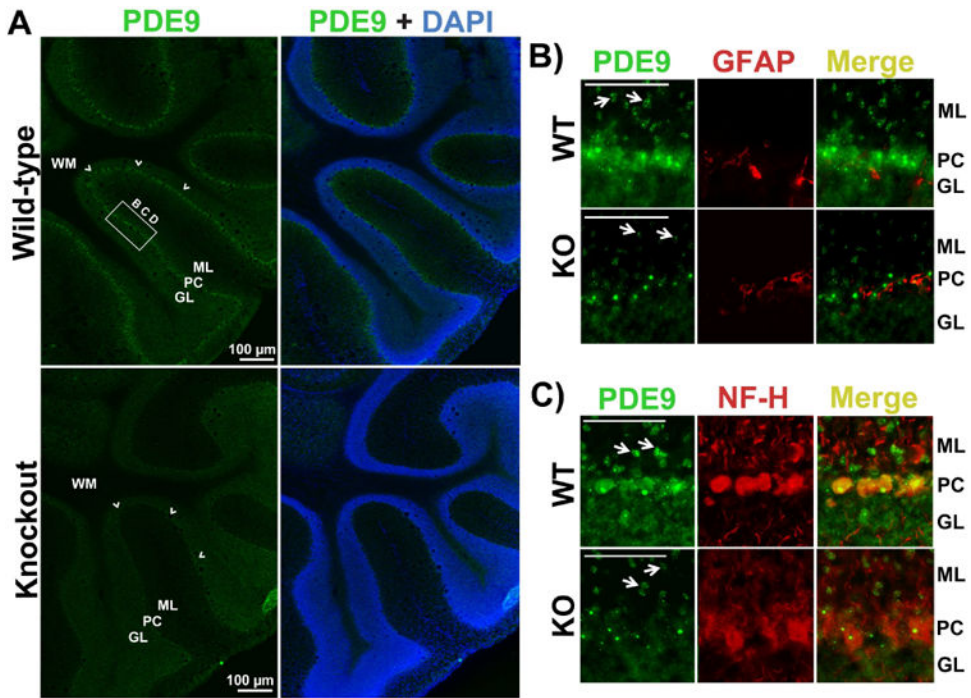
Figure 3.
PDE9 is enriched in the Purkinje cell layer of the cerebellum in adult brain tissue. Sagittal sections were taken from 4 month-old *Pde9a* wild-type (WT) and knockout (KO) mice and stained for PDE9A (green; antibody 13128-5), nuclei (DAPI; blue), and a either a marker for astrocytes (glial fibrillary acidic protein, GFAP; red) or neurofilaments (NF-H; red). A) A low magnification of the cerebellum shows that staining for PDE9A is stronger in the Purkinje cell layer (PC; outlined by arrow heads) and—to a lesser extent—the granular layer (GL) and molecular layer (ML) of a *Pde9a* WT vs KO mouse, arguing for specificity of the signal. The specific PDE9A signal is particularly discernable when comparing the PDE9A + DAPI merged images of the WT vs KO. B) Higher magnification of the sections shown in panel A reveals that PDE9A protein expression does not colocalize with the astrocyte marker GFAP. C) In contrast, PDE9A does colocalize with NF-H in Purkinje cell bodies; although, not NF-H in axons. PDE9A also appears to be specifically expressed in small cell bodies within the ML (arrows) and GL, which would correspond to inhibitory interneurons in the ML and granule and/or golgi cells in the GC. PDE9A staining does not appear to exhibit any dendritic-like or axon-like patterns. Note, the punctate signal present in the nucleus is non-specific as it is present in both the *Pde9a* WT and KO. Inset scale bars = 100 µm. Histogram stretch and gamma adjustments applied uniformly across *Pde9a* WT and KO sections for graphical clarity of images.
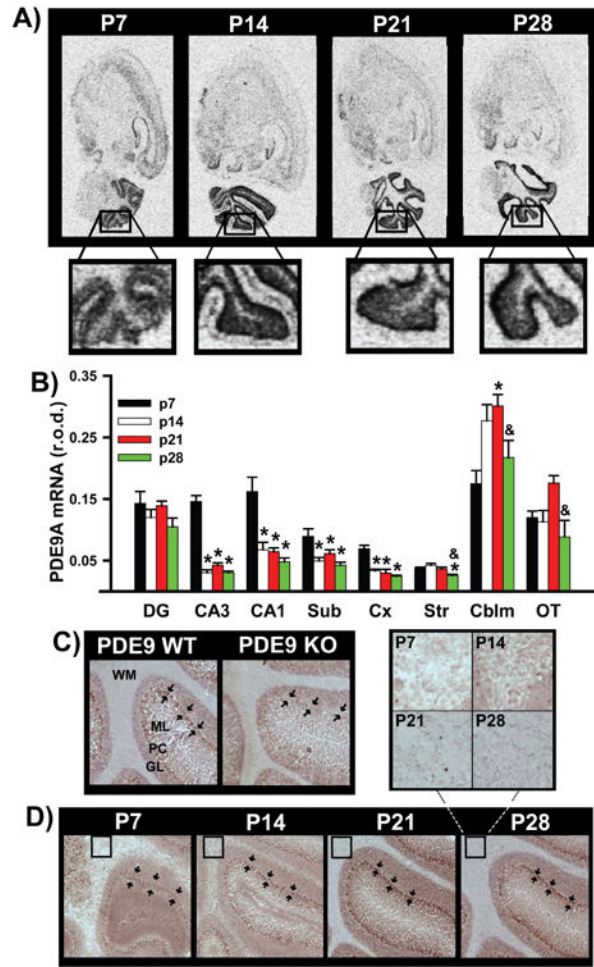
Figure 4.

The expression levels and distribution pattern of *Pde9a* mRNA and protein change during early postnatal development. A) Autoradiographs of PDE9A mRNA in C57BL/6J mice show that B) *Pde9a* mRNA expression significantly decreases between postnatal day 7 (P7) and P28 in CA3 ($F(3,18)=98.99$, $P<0.001$), CA1 ($F(3,18)=15.78$, $P<0.001$), subiculum (Sub; $F(3,18)=7.64$, $P=0.002$), somatosensory cortex (Cx; $F(3,18)=18.52$, $P<0.001$), and caudate-putamen (CPu; $F(3,18)=7.1$, $P=0.002$). In contrast, *Pde9a* mRNA expression in the cerebellum (Cblm) and olfactory tubercle (OT) peaks at P21 and then declines at P28 (Cblm: $F(3,15)=5.33$, $P=0.011$; OT: $F(3,18)=3.99$, $P=0.024$). Close inspection of the autoradiographic image suggests that the distribution of PDE9A mRNA across cerebellar layers may also change between P7 and P28. C) To test this at the protein level, we optimized conditions for immunohistochemistry (antibody 13128-5) using tissue from adult PDE9A wild-type (WT) and knockout (KO mice; note some background labeling is still present) and then D) labeled tissue from the above noted C57BL/6J mice. A redistribution of PDE9A protein was observed across cerebellar layers. The expression of PDE9 protein during early postnatal development appears to shift from the molecular layer (ML) and white matter (WM; highlighted by inset squares) to the Purkinje cell layer (highlighted by flanking rows of arrows). Caution should be taken when interpreting this expression,

however, since age-matched KO tissue was not available for study. Data collected with both the 13128-5 and 13128-6,7 antibodies.P7: n=4/region; P14-28: n=6/age/region except for Cblm P14: n=3. *Post hoc* *vs. P7, P<0.035-0.001; [&]vs. P21, P=0.041-0.011.
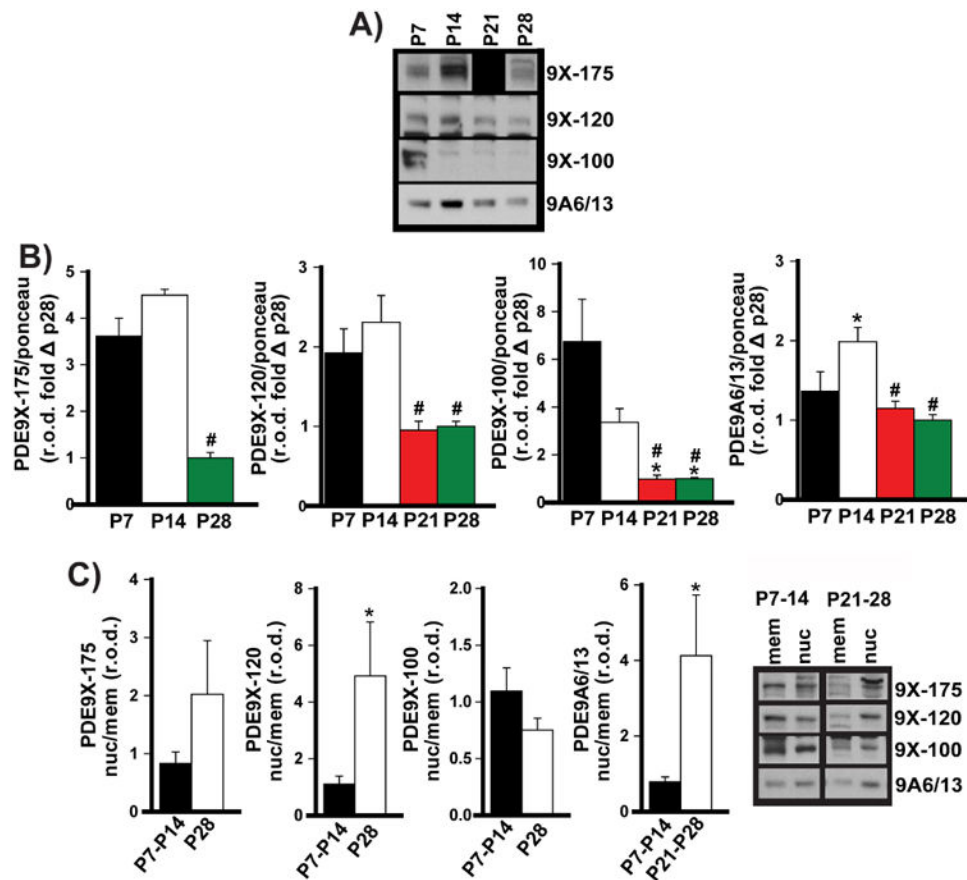
Figure 5.
The expression and compartmentalization of PDE9 isoforms dramatically change during early postnatal development in cerebellum. PDE9 was assessed in 2 cohorts of C57BL/6J mice. Cohort 1 included P7, P14, P21 and P28 and was probed using the 13128-5 antibody; whereas, cohort 2 only included P7, P14, and P28 (due to a limited number of available mice) and was probed using 13128-6,7. Unfortunately, PDE9X-175 was not reliably detected in total homogenates of cohort 1, and none of the novel isoforms were detected in the fractions from Cohort 1; therefore, no data for these isoforms were collected at P21. For bands that were detected across cohorts, effects were consistent so combined analyses are shown here. A) In total homogenates of cerebellum, expression of PDE9X-175 (on ranks: H(2)=8.32, P=0.001); PDE9X-120 (on ranks: H(3)=14.55, P=0.002), and PDE9X-100 (on ranks: H(3)=19.42, P<0.001) dramatically decreases between P7-14 and P28. In contrast, PDE9A6/13 increases between P7 and P14 and then decreases through P28 (F(3,22)=7.92, P<0.001) B) Further, PDE9X-120 (t(7)=-2.90, P=0.023) and PDE9A6/13 (rank test: T(23)=203.00, P=0.001) dramatically shift from a membrane-enriched to a nuclear-enriched distribution between P7-P14 and P21-P28. Note: PDE9A expression data for total homogenates were normalized to their ponceau stain as an indicator of total protein because GAPDH expression significantly increased during this period (see Supplemental Figure 2). Panel A: P7 and P28, n=6/age; P14 and P21, n=7/age, except for 9X-175 where n=3/age. Panel B 9A6/13: P7-14, n=14; P21-28, n=11. Panel B all other isoforms: P7-14, n=6/age;

P28, n=3. *Post hoc* *vs. P7, P 0.05-0.001; #vs. P14, P<0.05-0.001. Brightness and contrast adjusted for graphical clarity of blot images.
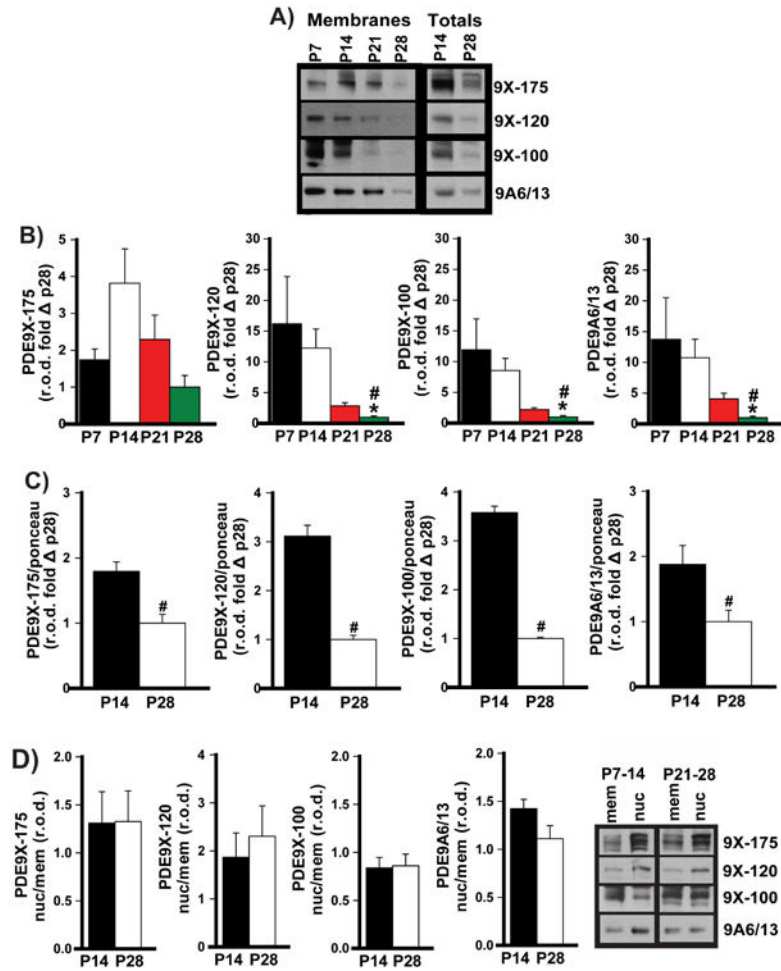
Figure 6.
Although expression dramatically decreases, compartmentalization of PDE9 isoforms remains relatively stable in hippocampus during early postnatal development. In C57BL/6J mice, A) PDE9 protein expression in hippocampus membranes of Cohort 1 (left; antibody 13128-5) and total homogenates of Cohort 2 (right; antibody 13128-6,7) mirror findings at the mRNA level. B) In membrane fractions, PDE9X-120 (on ranks: H(3)=12.15, P=0.007), PDE9X-100 (on ranks: H(3)=15.02, P=0.002), and PDE9A6/13 (on ranks: H(3)=12.41, P=0.006) significantly decrease from P7 to P28. PDE9X-175 shows a strong trend towards an effect of age, as well (F(3,17)=3.16, P=0.052). Note: membrane fractions were tested here as total homogenates had been depleted by previous experiments (see (Hegde et al., 2016a)). C) Similarly, expression of PDE9X-175 (t(6)=3.99, P=0.007), PDE9X-120 (t(6)=8.75, P<0.001), PDE9X-100 (t(6)=19.44, P<0.001); and PDE9A6/13 (t(6)=2.58, P=0.042) are all significantly reduced in total homogenates of P28 vs. P14 samples. Note: PDE9A expression data for total homogenates were normalized to their ponceau stain as an indicator of total protein because GAPDH expression dramatically increased during this period (see Supplemental Figure 2). C) In contrast to findings in cerebellum, no significant changes are noted between P14 and P28 in the compartmentalization of PDE9 isoforms in hippocampus of Cohort 2. Panel B: P7, n=4/age; P14 and P21, n=6/age; P28, n=5/age. Panel

C: n = 4/age. Panel C, n=3/age. *Post hoc* *vs. P7, P<0.05; #vs. P14, P<0.05-0.001. Brightness and contrast adjusted for graphical clarity of blot images.
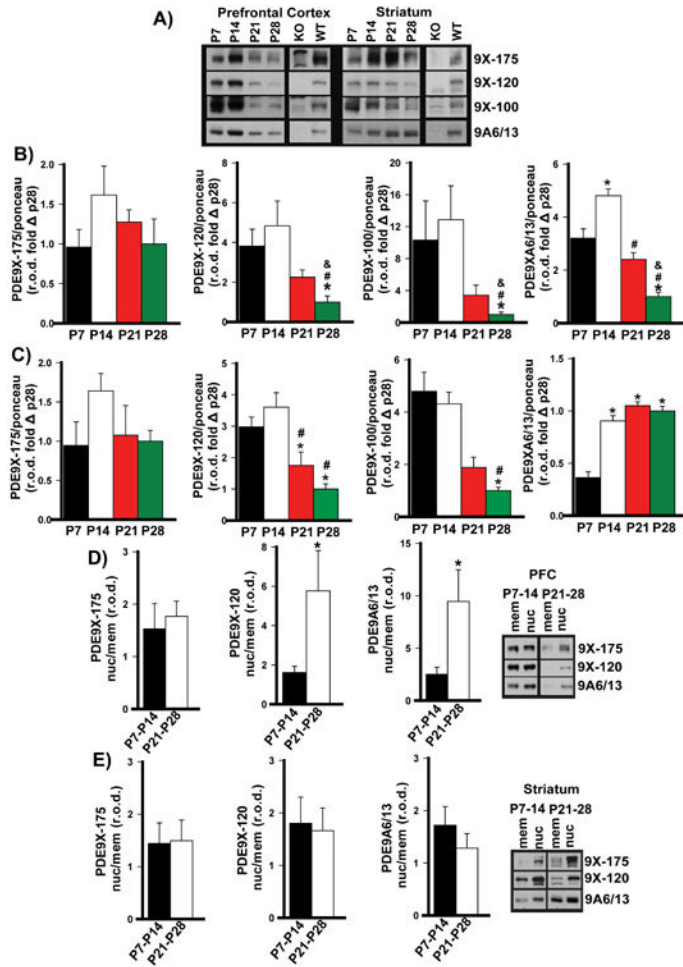
Figure 7.
All four PDE9 isoforms are also found in prefrontal cortex and striatum, with expression and compartmentalization that changes during early postnatal development of C57BL/6J mice. A) In cohort 1, expression (antibody 13128-5) of PDE9X-120 (on ranks: H(3)=11.54, P=0.009) and 9X-100 (on ranks: H(3)=9.75, P=0.021) significantly decrease between P14 and P28 in prefrontal cortex. In contrast, PDE9A6/13 expression exhibits an inverted-U shape, with an increase from P7 to P14 followed by a subsequent decrease in expression (F(3,12)=36.19, P<0.001). B) Across cohorts 1 and 2, (antibodies 13128-5 and 13128-6,7, respectively), expression of PDE9X120 (F(2,20)=13.25, P<0.001) and PDE9X-100 (on ranks: H(3)=17.76, P<0.001) also decline between P14 and P28 in striatum. In stark contrast, however, PDE9A6/13 expression increases between P7 and 14 in striatum (F(3,20)=35.02, P<0.001). C) In prefrontal cortex, the compartmentalization of PDE9 isoforms also changes between P7 and P28. Both PDE9X-120 (rank t-test: T(14)=49, P=0.05) and PDE9A6/13 (rank t-test: T(14)=46, P=0.021) shift from an equally-enriched to a nuclear-enriched distribution between P7-P14 and P21-P28. D) In striatum, no such systematic change in PDE9 compartmentalization appears to occur, with high variability in nuclear:membrane ratios seen across subjects. Note: PDE9A expression data for prefrontal cortex and striatum were normalized to their ponceau stain as an indicator of total protein

because GAPDH expression dramatically increased in these 2 brain regions during this period (see Supplemental Figure 2). Panel A,C: n=4/age; Panel B,D: P7, n=5; P14, n=7; P21, n=4; P28, n=8. *vs P7, P<0.05-0.001; [#]vs P14, P 0.05-0.001; [&]vs P21, P 0.05-0.003. Brightness and contrast adjusted for graphical clarity of blot images.
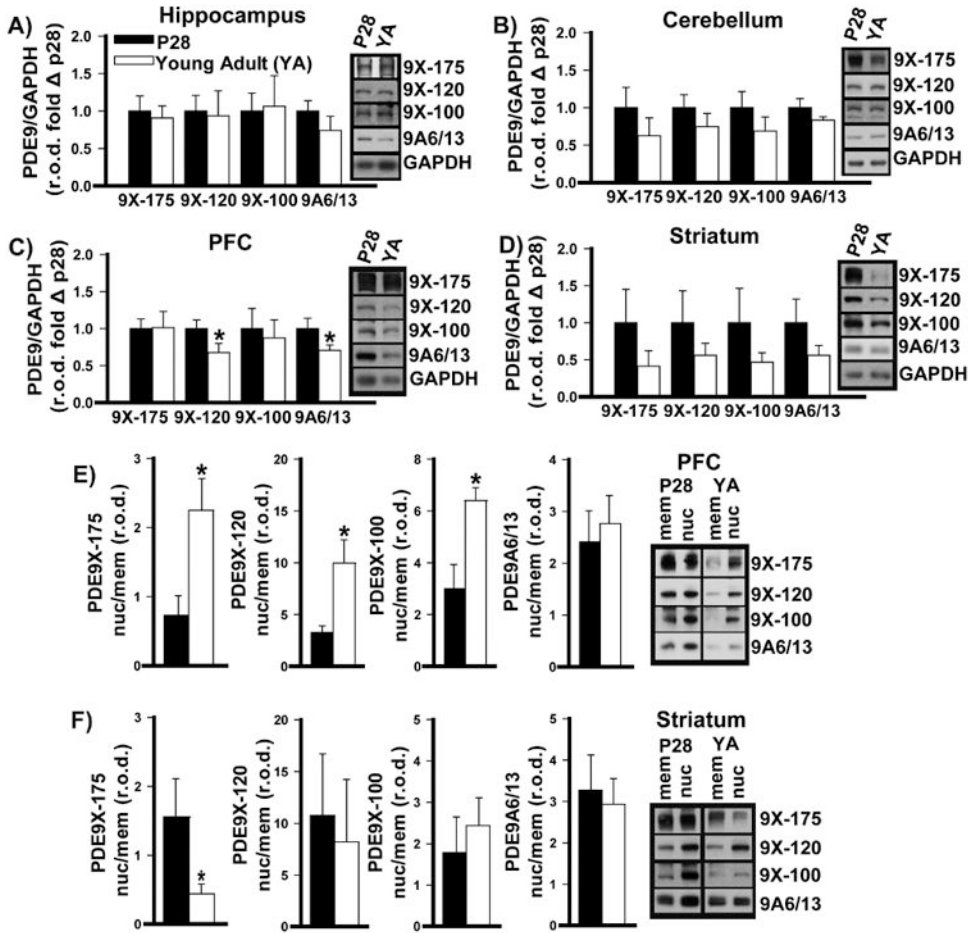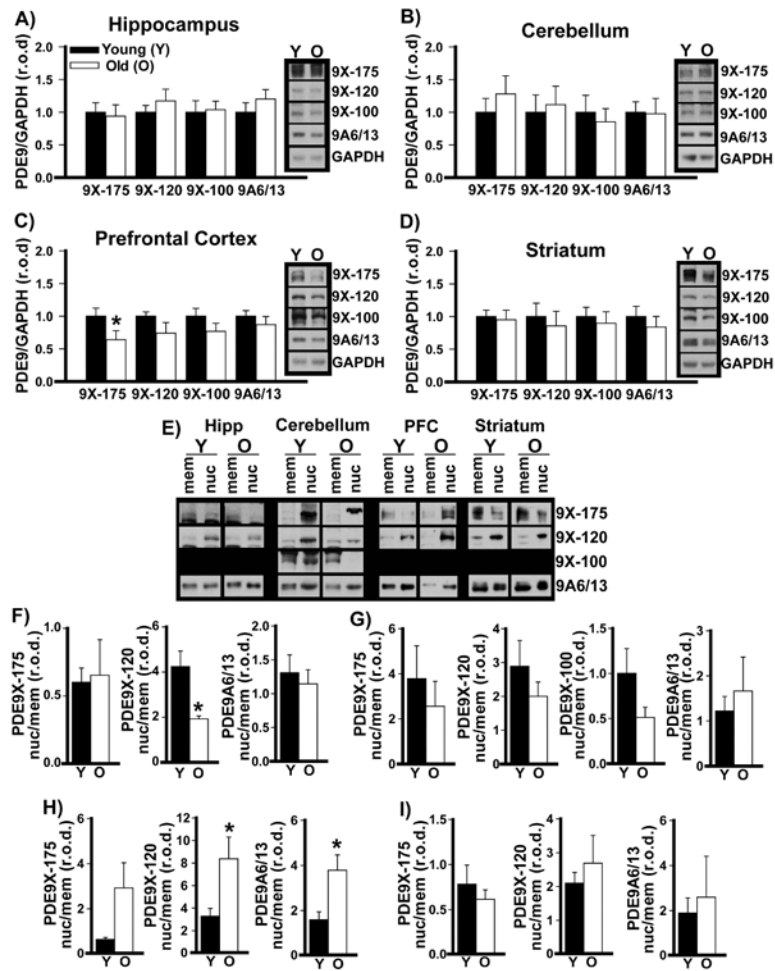
Figure 8.
PDE9A expression and compartmentalization continue to change between P28 and young adulthood in prefrontal cortex (PFC) and striatum but not hippocampus or cerebellum of C57BL/6J mice. A) Expression of all PDE9 isoforms remains stable in both hippocampus and B) cerebellum of C57BL/6J mice from P28 to young adulthood (YA). C) In contrast, PDE9X-120 (t(5)=5.07, P=0.004) and PDE9A6/13 expression continue to decline with age in PFC (rank t-test: T(10)=-21, P=0.031). D) No significant effects on PDE9 expression were observed in striatum due to high variability. E) PDE9 compartmentalization also continues to change in PFC, with PDE9X-175 (t(9)=-2.68, P=0.025), PDEX-120 (rank t-test: T(9)=18, P=0.03) and PDE9X-100 (t(9)=-3.38, P=0.008) becoming even more enriched in the nucleus vs membrane between P28 and young adulthood. F) Surprisingly, PDEX-175 shows the opposite pattern in striatum, shifting from the nucleus to the membrane (rank t-test: T(10)=17, P=0.017). Each blot was probed with antibody 13128-5. Note: there were no differences in GAPDH expression between ages. YA = 2-4 months old. n=6/age. *vs. P28, P=0.031-0.004. Brightness and contrast adjusted for graphical clarity of blot images.

Figure 9.
PDE9A expression and compartmentalization continue to change between young adulthood and old adulthood in prefrontal cortex (PFC) and hippocampus (Hipp) of C57BL/6J mice. There is no change in PDE9 isoform expression in total homogenates of A) hippocampus or B) cerebellum between young and old adulthood. C) In total homogenates of PFC, PDE9X-175 expression is significantly lower in old vs young adults (t(7)=2.65, P=0.033). D) There is no change in PDE9 isoform expression in total homogenates of striatum. E) PDE9 subcellular localization was also assessed. F) In hippocampus, PDE9X-120 appears to shift, becoming less enriched in the nuclear vs. membrane fraction (t(6)=3.30, P=0.016). G) In cerebellum, PDE9X-100 shows this same pattern in 4 out of the 5 replicates, but the effect did not reach statistical significance. H) In contrast, PDE9X-120 (t(12)=-2.19, P=0.049) and PDE9A6/13 (t(13)=-2.74, P=0.017) in PFC become even more enriched in the nuclear vs membrane fraction. I) Striatum shows no age-related changes in PDE9 subcellular compartmentalization. Data collected with both the 13128-5 and 13128-6,7 antibodies. Note: there were no differences in GAPDH expression between ages. Cerebellum, n=6/age; Hipp, n=4/age; PFC, n=8/age for totals and 7/age for fractions; Striatum, n=8/age. *vs young adult, P=0.049-0.016. Brightness and contrast adjusted for graphical clarity of blot images.
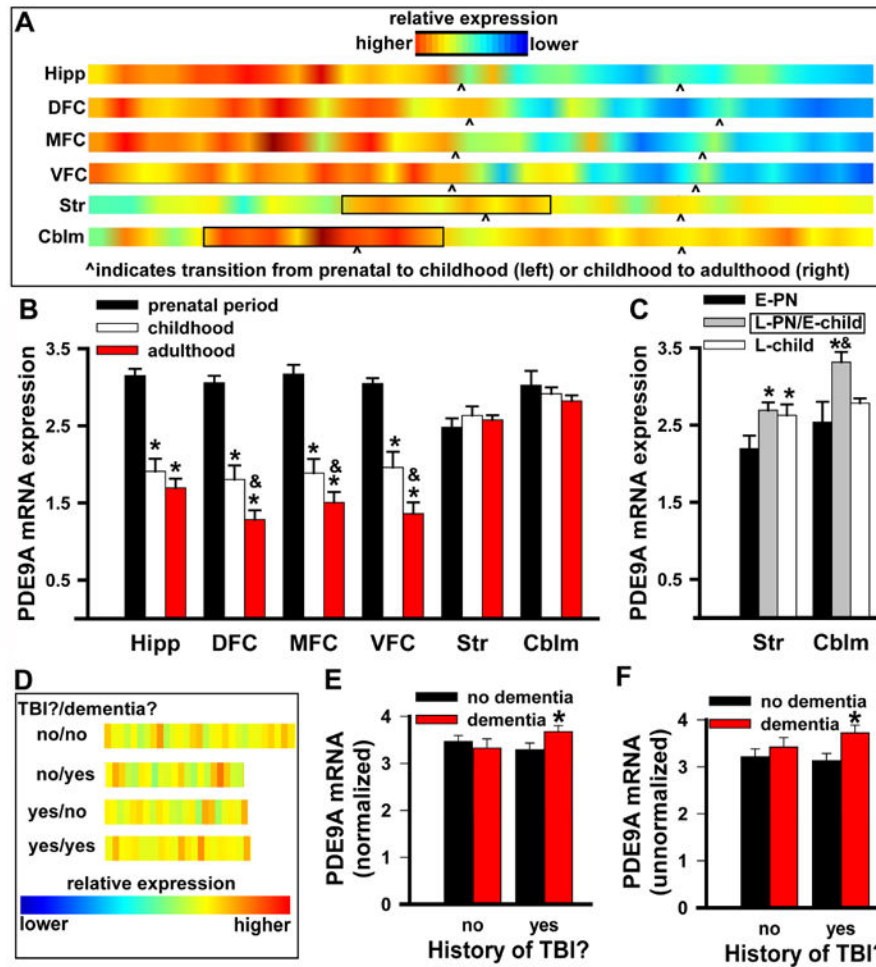
Figure 10.
PDE9A mRNA expression in humans mirror findings in mouse. To measure PDE9A expression across development in the human brain, data were collected from the © 2014 Allen Institute for Brain Science BRAINSPAN Atlas of the Developing Human Brain. A) Heatmaps showing PDE9A mRNA expression for each individual arranged from youngest (left) to oldest (right) and B) graphs of summed PDE9A mRNA expression clearly show a dramatic decrease in PDE9A mRNA expression in hippocampus (Hipp), dorsolateral prefrontal cortex (DFC), medial prefrontal cortex (MFC), and ventrolateral prefrontal cortex (VFC) between the prenatal period and childhood ($F_{(10,138)}=19.71$, $P<0.001$). Although there was not a significant difference in PDE9A mRNA expression in striatum (Str) or cerebellum (Cblm) between the prenatal period and childhood, a C) a *post hoc* analysis comparing the early prenatal period (E-PN;   16 weeks) vs. the later prenatal/early childhood period (period indicated by black rectangle: L-PN, >16 weeks; E-child, <1 year) vs later childhood period (l-child; >1year old) showed a significant effect of age in the striatum ($F_{(2,20)}=3.95$, $P=0.038$) and cerebellum ($F_{(2,21)}=8.78$, $P<0.002$), with patterns that were reminiscent of our findings in mouse. D) The Allen institute also measured gene expression in the hippocampus of adults aged 75-100+ to determine if a history of traumatic brain injury (TBI) and/or dementia would influence expression (© 2016Allen Institute for Brain

Science Aging, Dementia and TBI study). Heatmaps of normalized PDE9A expression for each individual as well as summed graphs of both E) normalized ($F_{(1,37)}$=4.63, P=0.038) and F) unnormalized data ($F_{(1,38)}$=5.02, P=0.031) show that individuals (males and females) with a history of traumatic brain injury (TBI) and a diagnosis of dementia exhibit a small but significant increase in PDE9A mRNA expression in hippocampus relative to individuals with a history of TBI but no diagnosis of dementia. There was no effect of dementia on PDE9A mRNA expression levels in absence of a history of TBI. prenatal, n=11-17/region; child, n=7-13/region; adult, n=7-8/region; no TBI/no dementia, n=29; no TBI/dementia, n=21; yes TBI/no dementia, n = 22; yes TBI/dementia, n = 22. *vs. prenatal, E-PN, or no dementia, P<0.04-0.001; [&]vs. child, P=0.03-0.004.

Table 1

Molecular weight (MW) of published human PDE9A (hPDE9A) isoforms.

PDE9A isoform	bp	aa	MW (kDa)
A1[&]	1779	593	68.5
A18[&]	1701	567	65.7
A17[&]	1656	552	64.1
A5[&]	1620	540	62.5
A2[^]	1599	533	61.7
A16[&]	1578	526	61.2
A9	1521	507	58.9
A13	1473	491	57.4
A6	1476	492	57.3
A3	1398	466	54.4
A4	1395	465	54.1
A12	1377	459	53.5
A10	1299	433	50.7
A7[*], A8[*&], A14[*], A19[*&], A20[*&]	1158	386	45.3
A11[#], A15[#]	1128	376	44.1

There are at least 20 different known variants of PDE9A due to alternative splicing and translation start sites (Rentero et al., 2003). The number of base pairs (bp), amino acids (aa), and the corresponding molecular weight (MW) have been noted here for each variant from largest to smallest. Molecular Weights were calculated using sequence gateway based on the CCDS for human PDE9A variants reported on NCBI (ncbi.nlm.nih.gov/gene/5152).

[*,#] indicates isoforms that have different 5′ UTR's, but same CCDS.

[^] -most homologous to the isoform currently regarded as "full length" rat and mouse PDE9A (Van Staveren et al. 2002).

[&] -includes exon 3b, 4b or 5, which are unique to human

Table 2

The expression and compartmentalization of PDE9 is isoform-, age-, and brain-region specific

	P7 to P28 (m) or prenatal to child (h)		P28 to young adult (m) or child to adult (h)		young adult to old (m)	
	expression	in relative enrichment	expression	in relative enrichment	expression	in relative enrichment
Hippocampus						
mRNA	↓	no	no	?	?	?
X175	∩	no	no	?	no	no
X120	↓	no	no	?	no	mem←nuc
#X100	↓	no	no	?	no	?
A6/13	↓	no	no	?	no	no
Cerebellum						
mRNA	∩	WM/ML→GC/PC	no	?	?	?
&X175	↓	no	no	?	no	no
*,&X120	↓	mem→nuc	no	?	no	no
&X100	↓	no	no	?	no	mem←nuc
*,&A6/13	∩	mem→nuc	no	?	no	no
Prefrontal Cortex						
mRNA	↓	no	↓	?	?	?
X175	no	no	no	mem→nuc	→	no
X120	↓	mem→nuc	↓	mem→nuc	no	mem→nuc
X100	↓	?	no	mem→nuc	no	?
A6/13	∩	mem→nuc	↓	no	no	mem→nuc
Striatum						
mRNA	↓(m)↑(h)	no	no	?	?	?
X175	no	no	no	mem←nuc	no	no
X120	↓	no	no	no	no	no
X100	↓	?	no	no	no	?
A6/13	←	no	no	no	no	no

*Expression is significantly higher vs. hippocampus

&Expression level expressed as fold change ( ) hippocampus significantly differs between isoforms

#Extent of enrichment in nuc vs membrane significantly is greater than other hippocampal isoforms

(m)--mouse; (h)--human;?--not assessed or not reliably detected on that blot; ∩-inverted-'U' shape; WM--white matter; ML--molecular layer; GC--granule cell layer; PC--Purkinje cell layer